Available online at www.sciencedirect.com
ScienceDirect
Trans. Nonferrous Met. Soc. China 30(2020) 2001−2034
Transactions of Nonferrous Metals Society of China
www.tnmsc.cn

A review of particulate-reinforced aluminum matrix composites fabricated by selective laser melting

Pei WANG[1,2], Jürgen ECKERT[3,4], Konda-gokuldoss PRASHANTH[3,5,6], Ming-wei WU[7], Ivan KABAN[2], Li-xia XI[2,8], Sergio SCUDINO[2]

1. Additive Manufacturing Institute, Shenzhen University, Shenzhen 518060, China;
2. Institute for Complex Materials, IFW Dresden, D-01069 Dresden, Germany;
3. Erich Schmid Institute of Materials Science, Austrian Academy of Sciences, A-8700 Leoben, Austria;
4. Department of Materials Science, Montanuniversität Leoben, A-8700 Leoben, Austria;
5. Department of Mechanical and Industrial Engineering, Tallinn University of Technology, 19086 Tallinn, Estonia;
6. CBCMT, School of Mechanical Engineering, Vellore Institute of Technology, Vellore-632 014, Tamil Nadu, India;
7. Department of Materials and Mineral Resources Engineering, Taipei University of Technology, Taipei 10608, China;
8. College of Materials Science and Technology, Nanjing University of Aeronautics and Astronautics, Nanjing 210016, China

Received 12 May 2020; accepted 7 July 2020

Abstract: Selective laser melting (SLM) is an emerging layer-wise additive manufacturing technique that can generate complex components with high performance. Particulate-reinforced aluminum matrix composites (PAMCs) are important materials for various applications due to the combined properties of Al matrix and reinforcements. Considering the advantages of SLM technology and PAMCs, the novel SLM PAMCs have been developed and researched in recent years. Therefore, the current research progress about the SLM PAMCs is reviewed. Firstly, special attention is paid to the solidification behavior of SLM PAMCs. Secondly, the important issues about the design and fabrication of high-performance SLM PAMCs, including the selection of reinforcement, the influence of parameters on the processing and microstructure, the defect evolution and phase control, are highlighted and discussed comprehensively. Thirdly, the performance and strengthening mechanism of SLM PAMCs are systematically figured out. Finally, future directions are pointed out on the advancement of high-performance SLM PAMCs.
Key words: selective laser melting; aluminum matrix composites; solidification behavior; microstructure; properties

1 Introduction

Additive manufacturing (AM) is a relatively new concept of the manufacturing processing based on the computer technology, which lies in stark contrast to traditional subtractive manufacturing processes [1−4]. Based on this concept, complex parts applied in different industries (e.g., aerospace industry, automotive industry, food industry, and medical industry) can be produced by different additive manufacturing technologies simultaneously without the tedious post-processing [5,6]. Selective laser melting (SLM) is considered as one of the

Foundation item: Project (GJHZ20190822095418365) supported by Shenzhen International Cooperation Research, China; Project (2019011) supported by NTUT-SZU Joint Research Program, China; Project (2019040) supported by Natural Science Foundation of Shenzhen University, China; Project (JCYJ20190808144009478) supported by Shenzhen Fundamental Research Fund, China; Project (ZDYBH201900000008) supported by Shenzhen Bureau of Industry and Information Technology, China
Corresponding author: Pei WANG; Tel: +86-755-26536224; Fax: +86-755-26557471; E-mail: peiwang@szu.edu.cn
DOI: 10.1016/S1003-6326(20)65357-2

promising powder-bed additive manufacturing technologies for metals and their matrix composites [7−10], whose working schematic is shown in Fig. 1. Firstly, SLM uses a 3D computer-aided design (CAD) model as a digital source of a part to be produced by an SLM device. In the second stage, i.e., the SLM processing, a thin layer of powder is deposited over the base plate by a special recoater, and then the high-intensity laser as an energy source is utilized to fully melt and fuse the selective regions of powder-bed dictated by the sliced CAD data. After completion of this melting and solidification for one layer, the base plate is lowered by a pre-set layer thickness, and the next powder layer is deposited on the precedent layer. By such layer-by-layer processing, the entire part with a complex geometry is fabricated completely and the final part would be obtained by suitable post-treatment (e.g., plasma polishing, mechanical polishing, electro-polishing and sandblast [11]) to meet the demand of the surface quality and dimensional accuracy.

According to the working principle of SLM, this technology has advantages of fabricating components with complex geometries compared with those manufactured by the conventional methods [8,12−14]. Moreover, the manufacture of the SLM components without using molds can also shorten the design and production time [15]. Therefore, in the recent years, more and more scientists and engineers have started to investigate the forming mechanism and performance of SLM alloys and its composites [16−18], and finally designed and fabricated the smart SLM components for special service conditions (e.g., implant parts, the runner mold, thin-walled blade ring of the aircraft engine, and the frame structure of automotive components, as shown in Fig. 2).

As the second most widely used metal surpassed only by steel and the most heavily consumed non-ferrous metal in the world, aluminum alloys play an important role in the industrial production and are applied to every aspect of our daily life (as listed in Table 1) [20−22]. Therefore, aluminum alloys have become one of the earliest alloys fabricated by SLM technology and studied by scientists since a few years ago when the researches on the SLM Al alloys were only carried out in the laboratory and the SLM market was quite new and small [23,24]. However, with the expansion of the market demand on the high-performance aluminum components integrated topology optimization, several SLM aluminum alloys and their parts have been produced and applied, resulting in a decrease in the current production costs [6,25−27]. For example, SLM Al−10Si−Mg (in wt%, the same hereafter) and Al−12Si alloys with good performance have been applied successfully in aerospace and automotive sectors (e.g., the vertical tailplane bracket, motorsports and aerospace interiors) [28,29]. Moreover, with the in-depth investigations on the SLM technologies (mainly about parameter optimization) and the forming mechanism of SLM Al alloys (mainly about the rapid solidification theory of Al alloys during the SLM processing) [30,31], in addition to the Si-rich Al alloys with good castability (e.g., Al−12Si [32,33], Al−10Si−

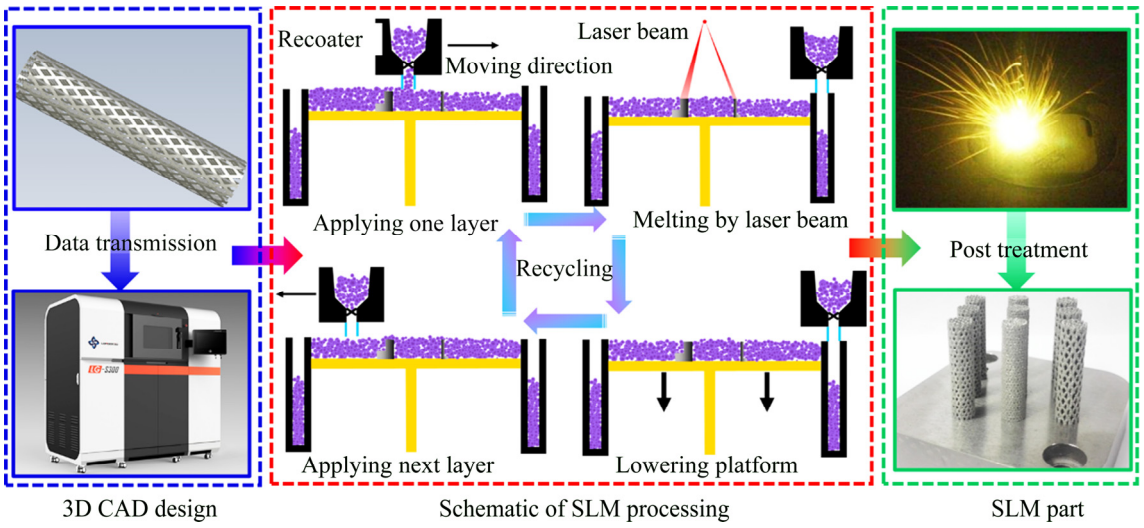

Fig. 1 Processing steps involved in SLM production from 3D design to final parts

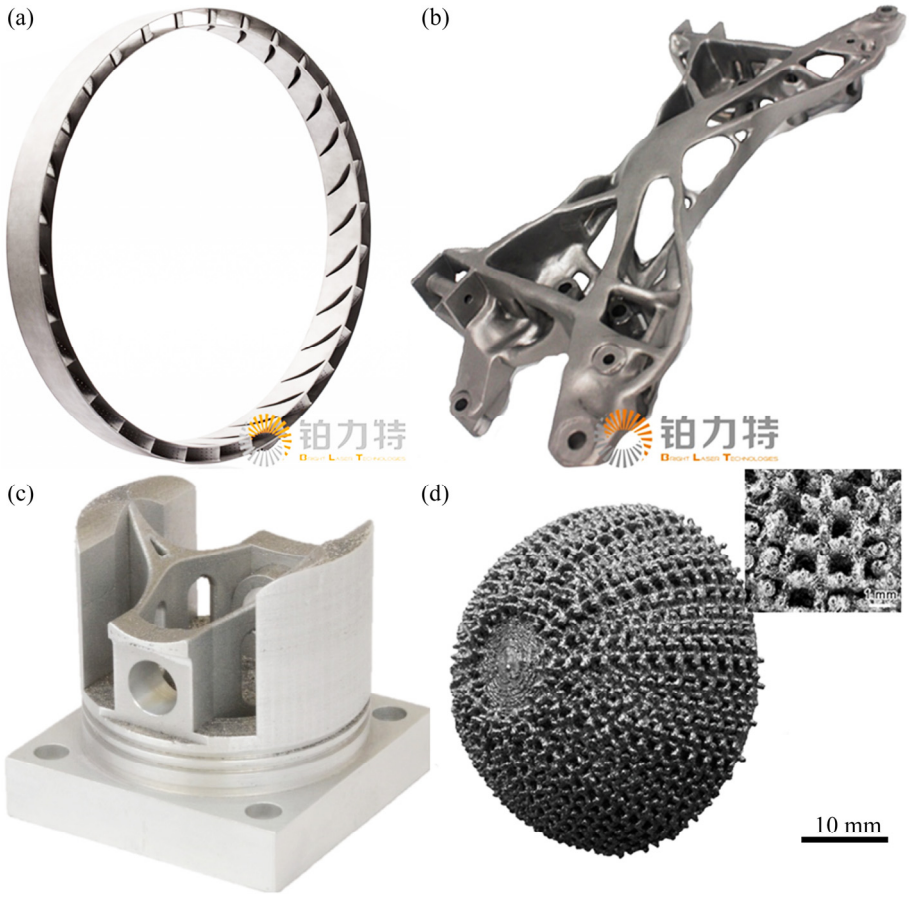

Fig. 2 Complex components with structural optimization applying in mold manufacturing, aerospace industry, and automotive industry: (a) Thin-walled blade ring of aircraft engine (supplied by Bright Laser Technologies Co., Ltd.); (b) Frame structure of automotive components (supplied by Bright Laser Technologies Co., Ltd.); (c) Piston [19]; (d) Acetabular cup [13]

Table 1 Classification of wrought aluminum alloys including their heat treatment and applications [20−22]

Series	Main alloying elements	Heat treatment	Application
1xxx	≤1%	Non-heat treatable	Electrical and chemical industries
2xxx	Cu	Heat treatable	Aircraft structures and automotive industry
3xxx	Mn	Non-heat treatable	Heat transfer, packaging, and roofing-siding
4xxx	Si	Non-heat treatable	Welding rods, and brazing sheet
5xxx	Mg	Non-heat treatable	Automotive, cryogenic, and marine
6xxx	Mg and Si	Heat treatable	Architectural extrusion, and automotive components
7xxx	Zn	Heat treatable	Aircraft structural components, and other high-strength fields
8xxx	Others (Li, Sn)	Heat treatable	Bearing, and connecting rod

Mg [34,35] and Al−9Si−3Cu [36]), other kinds of Al alloys, including 2xxx, 3xxx, 5xxx and 7xxx series alloys (e.g., Al−4.5Cu−2Mg−0.6Mn alloy [37], Al−3.5Cu−1.5Mg−1Si alloy [38], Al−Mg−Zr alloy [39,40], Al−Mn−Sc [26], Al−9.1Zn−2.3Mg−1.5Cu alloy [41] and Al7075 [42,43]), were also fabricated by SLM in recent years.

It is well known that Al alloys demonstrate lower strength, stiffness and wear resistance than other alloys [44−47]. Therefore, in order to develop the high-performance Al materials, the novel Al matrix composites (AMCs) developed and studied by numerous state-of-art technologies have always been attracting the research attentions [48−51]. The

particulate-reinforced aluminum matrix composites (PAMCs) are one attractive sort of the AMCs for the demands set by the industries as shown in Table 2 because of their excellent combination of low density, high specific strength, high stiffness, good wear performance and high corrosion resistance [53−57]. However, the demand of complex-shaped PAMC products in numerous industrial fields by the conventional fabrication methods of PAMCs (e.g., high energy ball mill mixing and sintering, stir casting, vacuum casting and squeeze casting) is required widely but is extremely difficult to meet [58−61]. Therefore, the smarter PAMCs with higher performance need to be designed and produced by SLM to better satisfy the requirements [62]. Based on the in-depth understanding of the SLM processing of Al alloys, SLM PAMCs started to be designed and investigated, which has gradually become a new hot research topic with the global focus in recent years [63−65]. However, due to the unique layer-by-layer processing mode and the complete-melting/rapid-solidification mechanism, SLM PAMCs exhibit a special non-equilibrium microstructure and a striking performance, which are different from the conventional PAMCs and need to be understood comprehensively. In addition, some critical issues have limited the densification of SLM PAMCs and the further improvement of their performance, which also needs to be analyzed and clarified thoroughly. Nevertheless, until now, less work has been reported comprehensively in the current work about SLM PAMCs and the forming mechanism, the microstructure evolution and the performance of these materials are seldom discussed.

As such, in this work, the recent efforts and advances in the SLM PAMCs are overviewed in order to reveal the potential mechanism. Based on the comprehensive understanding of these early works and our numerous original works, some important issues about the SLM PAMCs are discussed and emphasized. Firstly, the special attention is paid to the metallurgical behavior and synthesis principle of the SLM PAMCs during the SLM process. Afterward, the evolution of metallurgical defects and metallurgical micro-structures of SLM PAMCs are explained and presented to highlight the unique features different from those in the conventionally processed PAMCs. Secondly, the current issues that limit the fabrication of the high-performance SLM PAMCs are listed and analyzed, with the aim to clarify the important principle of SLM PAMCs, involving the selection of reinforcements, the feedstock preparation method, the defect control, and the phase control, and to guide the design and fabrication of the high-performance SLM PAMCs.

Table 2 Processing, properties, and application of some common Al matrix composites [48,52,56]

AMC	Processing	Property	Application
SiC/Al	Spark Plasma Sintering	HV 325	Piston rings, armor, and nozzle
Al_2O_3/Al	High energy ball mill mixing and sintering	$HV_{0.05}$ 93.9	Refractory, and structural field
Ti_3SiC/Al	Melt infiltration	HV 751 C_s=750 MPa	Space and defense industries
Graphene nanoplatelets/Al	Pressure infiltration	σ_s=250 MPa	Piston engines, wheels, and electric motor housing
Fly ash/Al−7Si−Mg	Stir/gravity casting	σ_s=45−62 MPa	Manifolds, and cylinder heads
Graphene/AA7050	Squeeze casting	σ_s=255 MPa	Aerospace and automotive industries
B_4C/AA6061	Vacuum casting	σ_s=340 MPa	Automotive, aerospace, military, and nuclear industries
TiB_2/A380	In-situ salt−metal reaction method	σ_s=160 MPa	Automobile and aerospace industries
SiC/A356	Rheocasting	HRB 73−93	Wear-resistant components, driveshaft, and brake rotors
TiC/AA1050	Accumulative roll bonding	σ_s=58 MPa	Structural, and automotive fields

σ_s—Ultimate tensile strength; C_s—Ultimate compressive strength

Thirdly, the properties of current SLM PAMCs (mainly mechanical properties and wear resistance which are the important performances of PAMCs for the industrial application) are listed to manifest the advantage of the SLM PAMCs, and then the relationship between the microstructure and properties is analyzed. In the final part, some prospective viewpoints about the design, the fabrication, and the fracture mechanism of SLM PAMCs are proposed for future work.

2 Solidification behavior of SLM PAMCs

2.1 Solidification theory of selective laser melting

Numerous works [66,67] have indicated that the SLM process has a similar solidification mode to fusion welding. Based on the solidification behavior of the laser welding, the solidification behavior and grain structure of a single laser track were studied and are shown herein to reveal the solidification mechanism of SLM materials (Fig. 3).

As described in the classical solidification theory on welding metallurgy [67,71], the idealized solidification mode, known as the competitive mechanism, may change from planar to cellular, columnar dendritic, and equiaxed dendritic across the scanning zone due to the decreasing ratio of G/V (G: temperature gradient; V: solidification rate) from the fusion line to the top of the melt pool (Fig. 3(a)). This solidification mode, especially columnar to equiaxed transition (CET), is used to explain the solidification behavior and micro-structures of SLM Al alloys (e.g., the cellular structure composed of eutectic Al−Si [72,73] and the lamellar structure composed of eutectic Al−Al_2Cu in SLM Al−33Cu alloy [74,75]). However, due to the random grain orientation of the grains generated in the precedent layer during the layer-by-layer processing, the SLM alloys usually have a recycling microstructure and grain orientation [76,77], which cannot be predicted completely and precisely by the classical qualitative welding theories [70,78]. In order to overcome this obstacle, LI and TAN [70] utilized the 3D meso-scale Cellular Automata model to simulate the meso-scale grain structure of SLM alloys successfully. Their results indicated that without any bulk nucleation (i.e., nuclei density is zero), the columnar grains are dominated in the grain structure (Figs. 3(a) and (b)) and prefer growing perpendicular to the moving solidification front (i.e., orange dashed line as indicated). But there is no evident equiaxed region at the top of the melt pool. Moreover, on the cross-section, the near-columnar shaped grains grow into the interior of the melt pool. However, with the increase in the nuclei density and/or a decrease in the critical undercooling, the top zone of the melt pool would facilitate the occurrence of equiaxed grains. Such a simulated grain map of the cross-section along the building direction is confirmed by the EBSD results reported by LIU et al [69] (as shown in Fig. 3(d)). Their experimental results also suggested that the variation of the grain structure is affected by the

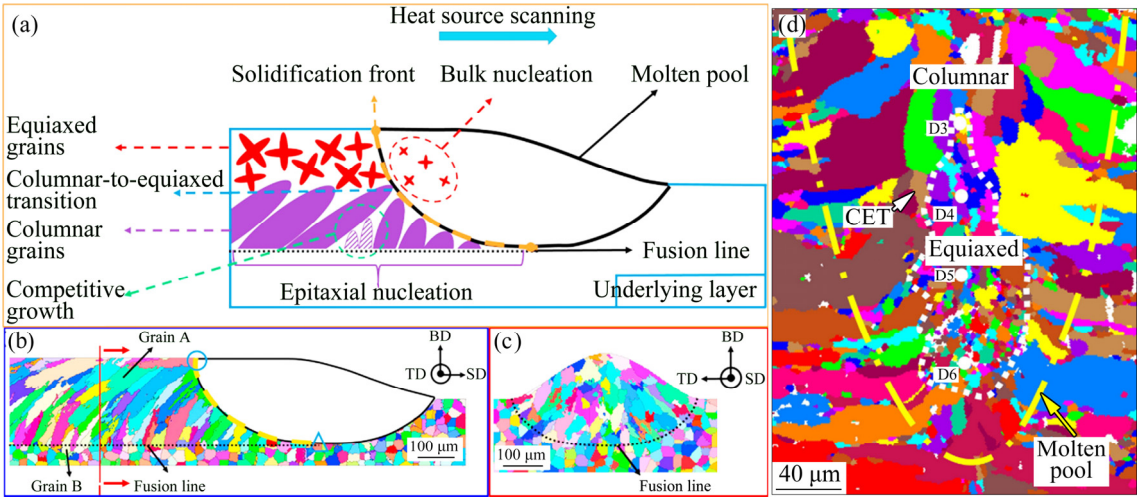

Fig. 3 Solidification behavior of center plane across scanning direction (a), simulation of single-pass grain structure of center plane across scanning direction (b), simulation of single-pass grain structure of cross-section along building direction (c), and grain map of cross-section along building direction measured by electron backscattered diffraction technology (EBSD) (d) [68−70]

scanning speed and the CET criterion of SLM Al−10Si−Mg alloy determined by the ratio of G/V. If the ratio of G/V is lower than a specific value, the CET transition occurs and equiaxed grains are generated, as shown in Fig. 3(d). Even though the present solidification theories are based on the SLM alloys but not specifically for composites, these works are significantly helpful to clarify the forming mechanism of the SLM composites and the formation of microstructure.

2.2 Diffusion and interaction of SLM PAMCs during laser melting

Based on the above fundamental solidification theory of SLM alloys, most solidification phenomena in the melt pool of SLM composites can be clarified. However, some special solidification phenomena in the melt pool of SLM composites cannot be ignored due to the influence of the reinforcement on the solidification behavior of the Al matrix. The addition of the reinforcement can cause the change of the nuclei density in the melt pool, the diffusion of the alloying elements to the matrix and the interaction between the reinforcement and the matrix. Generally, these special solidification phenomena can influence the defect evolution, the grain structure, the formation, and the distribution of the phases, which are the key factors to obtain the SLM composites with the stable and good performance. Due to easy operation, low cost and flexible design of the mixture, ball milling has become the common method to mix the powders of the reinforcement and matrix. Therefore, the schematic of the thermophysical phenomena around the melt pool during the SLM processing of PAMCs with the powder mixtures is depicted in Fig. 4.

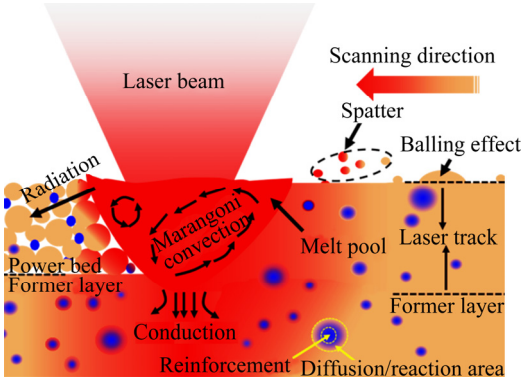

Fig. 4 Schematic of thermophysical phenomena around melt pool during SLM processing of PAMCs [79−81]

As shown in Fig. 4, when the laser beam irradiates the surface of the powder bed, a part of the laser energy is reflected and is absorbed by the powder [82]. The typical thermophysical phenomena (e.g., the laser radiation [83,84], the spatter of the small particle [85,86], the Marangoni effect [87], the balling effect [88] and the heat conduction [79]) can happen in the melt pool during the SLM processing of PAMCs, which are similar to the scenarios in the melt pool of SLM alloys. However, these phenomena in the SLM PAMCs display special features. For example, Marangoni flow can force the movement of the reinforcements and influence their distribution and morphologies in the Al matrix [89]. Moreover, because of the high temperature in the melt pool, some reinforcements can react with the Al matrix or some elements of reinforcements can diffuse into the matrix, thereby changing the chemical/physical properties of the Al matrix. In addition, the particulate reinforcements are randomly dispersed in between the matrix powder, as shown in Fig. 4, which are irradiated together by the laser. Therefore, due to the non-uniform distribution of the reinforcements in the matrix powders, the difference of the particle size and the absorptivity of the reinforcement from the Al matrix, the optimized parameters for the whole composites are not fit in a partial area, which can lead to the formation of defects in these zones [82,83].

In order to clarify the reaction and diffusion between reinforcements and matrix in the composites during the laser melting (Fig. 5), LOH et al [91] fabricated in-situ Al−Cu alloys by SLM from mixtures of Al−4.5Cu and Cu powders. Backscattered electron (BSE)-scanning electron microscope (SEM) images suggested that during the SLM process, the Cu powder and the Al−4.5Cu powder are melted locally due to the local high temperature up to 2200 K. However, due to the short lifetime of the melt pool (typically t<3 ms [91,92]) and the limited solute diffusivity in Al (D_L=3.5×10^{-9} m^2/s [93]), Cu cannot fully diffuse into the surrounding liquid Al matrix, leading to the formation of intermetallic phases between the Cu powders and Al matrix. Although the Cu solute diffusion into the Al matrix is restricted, the overlaps between tracks generated by the layer-by-layer processing would provide preferential diffusion paths to ensure the diffusion of Cu into the

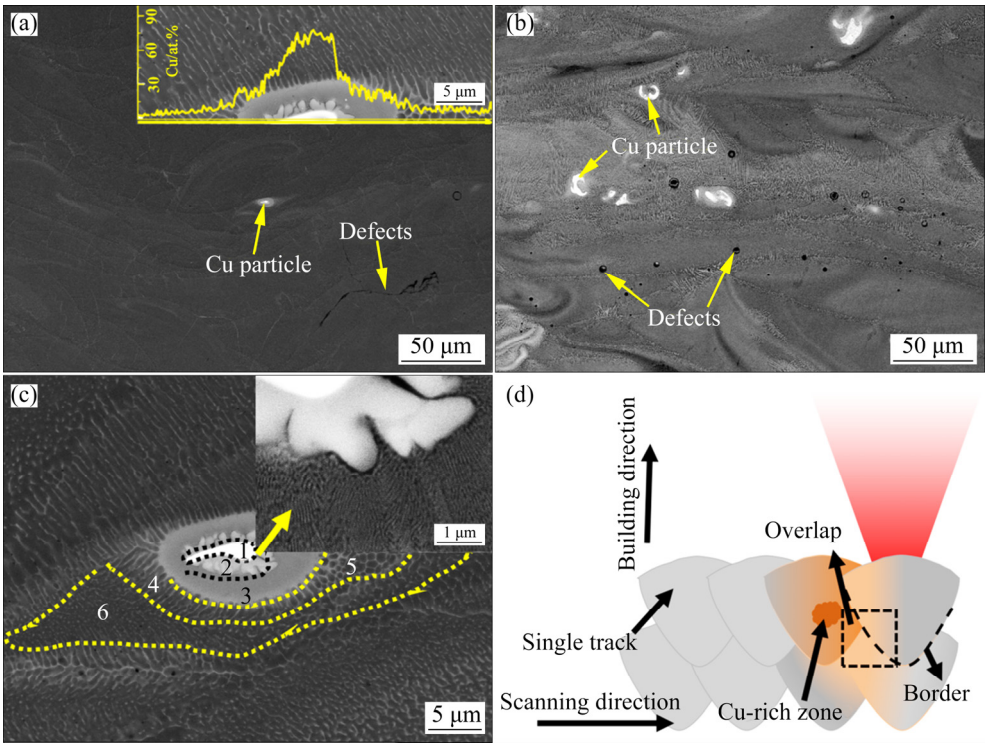

Fig. 5 BSE-SEM micrographs for SLM Al−*x*Cu alloys: (a) Al−6Cu alloy (inset: Cu distribution across Cu-rich zone); (b) Al−40Cu alloy; (c) Cu-rich zone in Al−6Cu alloy; (d) Schematic illustrating diffusion of Cu during SLM processing (Ref. [90])

adjacent areas, as depicted in Fig. 5(d). The similar diffusion and reaction phenomena of the reinforcements and matrix in SLM PAMCs are also observed and analyzed in the fabrication of SLM $Ti_{52.4}Al_{42.2}Nb_{4.4}Mo_{0.9}B_{0.06}$(TNM)/Al−12Si composites [94] and SLM Al−Fe−Cr quasicrystal (QC)/CP-Al composites [95].

It should be mentioned that, in some work, the in-situ salt−metal reaction method was used to prepare the raw powders for the SLM processing, which facilitates homogenous distribution of the reinforcement in the matrix and can avoid the problems introduced by the ball milling (such as the loss of the reinforcement, the change of the sphericity and size of the matrix powders, and the decreasing quality of the matrix powder) [96]. However, because of the relatively high cost and complex procedure of the in-situ salt−metal reaction method, this method was rarely used and is not depicted in Fig. 4 [97]. But the special microstructure and properties of the composites with the powders prepared by the in-situ salt−metal reaction method would be discussed in the coming sections.

2.3 Heterogeneous nucleation, equiaxed growth and grain refinement during processing of SLM PAMCs

As mentioned in Section 2.1, SLM Al alloys have mainly a columnar microstructure and CET transition only occurs when G and V satisfy a certain relationship [69]. However, for SLM PAMCs, the reinforcing phases (such as TiB_2, Al_2O_3, Si and SiC [98,99]) are often found to suspend in the melt pool or the reaction products (such as Al_3Zr, $TiAl_3$, VAl_{10} and $A1B_2$ [37,100]) between Al matrix and thus the reinforcing phases may serve as a preferred site for heterogeneous nucleation of primary phases crystallizing from the melt pool [98]. The increasing preferred sites are beneficial to the formation of the equiaxed structure. Moreover, the introduced reinforcing phase of SLM PAMCs can also increase the sufficient number of inoculants ahead of the advancing solid/liquid interface, which can promote the formation of the equiaxed structure [101].

According to the classical theory of the heterogeneous nucleation and grain growth [102], the novel SLM PAMCs with high performance are

designed and developed by the microstructure manipulation. For example, in order to fabricate the high-strength SLM Al−Zn materials, MARTIN et al [19] designed the Zr/Al7075 nanoparticles by the nanoparticle assembly as the metal feedstock as shown in Figs. 6(a) and (b). Compared to the cracks generated at the columnar grains of SLM Al7075 alloy, the addition of the Zr particles can lead to the equiaxed growth of Al grains and avoid the formation of the cracks between the grains in the SLM ZrH_2/Al7075 composite (Figs. 6(c−f)). In fact, the addition of zirconium does not change the solidification curve into a more favorable shape, as shown in Fig. 6(g). This indicates that the dramatic difference between the solidus temperature and liquidus temperature still can lead to the hot tear of the Al grains, which makes the SLM ZrH_2/Al7075 composite have a high tendency for cracking during the rapid solidification in this condition [103]. Therefore, the anomalous free-crack phenomenon in SLM ZrH_2/Al7075 composite should be attributed to the equiaxed growth of Al grain induced by the early inclusion of Zr. Moreover, the equiaxed growth can more easily accommodate the thermal contraction strains between the grains associated with solidification, ultimately resulting in an alloy system with high crack resistance. This explanation can be supported by the comparison of the morphologies of the SLM Al7075 alloy with cracks and the SLM ZrH_2/Al7075 composite without cracks (Fig. 6(h)). This paves a smart way to fabricate the crack-susceptible Al alloys and its composites. In fact, this is a meaningful principle breakthrough on the design of the novel SLM Al matrix materials, especially SLM PAMCs. As the equiaxed growth of Al grains during the rapid solidification can not only avoid the formation of cracks but also refine the grains, free-cracks and refined grains are the demands to achieve high-performance Al matrix composites by SLM. Therefore, the reasonable selection of the reinforcement is the key factor to fabricate novel SLM PAMCs with a high density and a good performance.

Similar works also confirm that the addition of Zr and Si particles introduced by the powder mixing can result in the formation of equiaxed growth of Al grains and elimination of cracks generated during rapid solidification [19,99,104], thereby significantly enhancing the mechanical properties of these SLM matrix alloy. Moreover, these results also indicated that the equiaxed Al grains can significantly decrease the anisotropy of the Al matrix and demonstrate similar mechanical

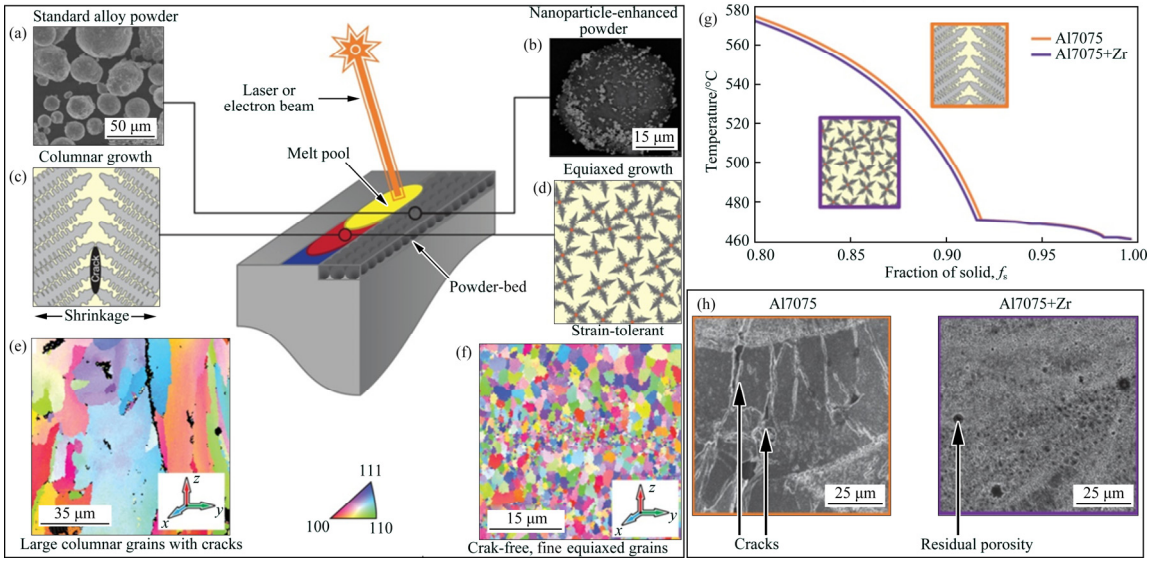

Fig. 6 Grain refinement and solidification behavior of SLM Al alloys [19]: (a) Conventional Al7075 powder feedstock; (b) Al7075 powder functionalized with nanoparticles; (c) Columnar growth of dendrites during laser melting; (d) Equiaxed grain growth induced by suitable nanoparticles during laser melting; (e) Inverse pole figure of columnar grains with periodic cracks of SLM alloys using conventional approaches; (f) Inverse pole figure of fine equiaxed grain without hot cracking using functionalized powder feedstock with nanoparticles; (g) Effect of zirconium on solidification behaviour of Al7075 and ZrH_2/Al7075 at high solid fractions; (h) SEM images of polished and etched specimens depicting microstructures with and without addition of zirconium

properties of PAMCs along different directions (i.e., the building direction and scanning direction) [105].

As expected for the reaction products of the Al matrix and the reinforcements, some reinforcements can also lead to the equiaxed growth of Al grains and grain refinements by themselves. For example, TiB_2, as a common grain refiner in Al alloys due to a preferable natural stacking sequence of Al atoms on TiB_2 [106,107], can cause the equiaxed growth and the grain refinements of Al grains without the apparent reactions [100,108]. XI et al [109] prepared the TiB_2/Al−12Si powder mixtures by ball milling and successfully fabricated the SLM TiB_2/Al−12Si composite. As shown in Fig. 7, compared with the large, recycling and elongated grains in the SLM Al−12Si alloy, the SLM TiB_2/Al−12Si composites have refined and equiaxed grains. It was also indicated that the introduction of TiB_2 particles into SLM Al−12Si alloy by ball milling is suitable to produce the additive metal feedstock used for the fabrication of the SLM TiB_2/Al−12Si composite [109] (and another composite such as TiB_2/Ti composite [111] as well).

3 Current issues of SLM PAMCs

3.1 Selection of reinforcements

How to select a suitable reinforcement is always the key to design high-performance PAMCs. Therefore, the selection of the reinforcements is the first issue of the fabrication of SLM PAMCs with high performance. It is well known that the content in SLM PAMCs, the particle size, the agglomeration, and the physical characteristics of the reinforcements have a significant effect on the processing and microstructure of SLM PAMCs. The research indicates that with increasing the content of ceramics, the generation of pores is more serious and the relative density of SLM PAMCs decreases dramatically [112]. The formation of pores results from the partial melting of particulate reinforcements and the heterogeneous dispersion of heat and mass caused by nonuniform distribution of particulate reinforcements at the micro-scale [112]. Similar phenomena have also been figured out in other metallic based composites [113]. Besides the fraction of the reinforcements, the agglomeration and physical characteristics of the reinforcements have a significant effect on the densification and microstructures of SLM PAMCs [114]. The agglomeration of the particles often occurs at the surface of the matrix powders, which can prevent the direct exposure of the matrix powder to the laser. Therefore, the existence of agglomeration can make the powder feedstocks more sensitive to SLM parameters, which increases the difficulty of the densification of the SLM PAMCs [115,116]. The addition of the reinforcements can drastically affect the physical characteristics, mainly laser absorptivity, of the powder feedstocks of SLM PAMCs [16], and the laser absorption is the key

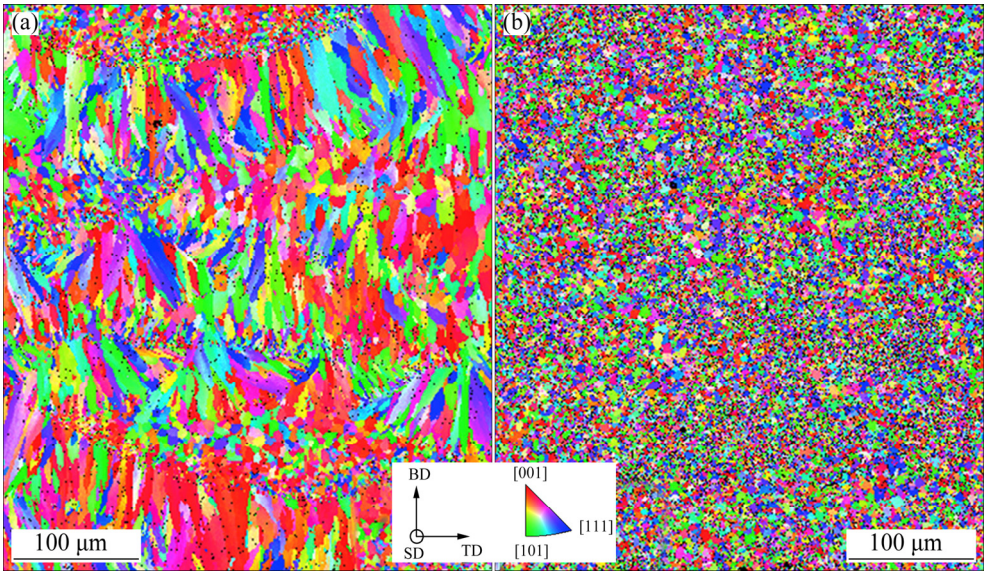

Fig. 7 Comparative EBSD grain orientation maps of SLM Al−12Si alloy (a) and SLM TiB_2/Al−12Si composites (b) of powder mixtures [109,110]

factor to the heat absorption and Marangoni flow which determine the processing parameters and the microstructure [117]. Therefore, clarifying the effect of the reinforcements on the laser absorptivity of the powder feedstocks is helpful to find the optimized parameters and explain the thermophysical phenomena of the melt pool.

Furthermore, the chemical/physical properties of the reinforcement (such as the coefficient of expansion and the melting point), the stability of the interface and the wetting behavior between the reinforcement and Al matrix are also crucial factors for the fabrication of PAMCs, because they determine the forming quality and mechanical properties of a composite [118]. However, for the SLM composites, due to the high temperature (>2000 K) of the melt pool during SLM process [119−121], thermophysical phenomena in the melt pool are more complicated and difficult to control than the processing of the conventional composites, as mentioned in Section 2.2. Therefore, it is important to clearly understand the thermophysical condition of the reinforcements in the melt pool during SLM process. The current method is to analyze the thermophysical characteristics during the SLM process with different processing parameters (e.g., laser absorptivity of the powders, laser spot radius, track numbers, laser power, scanning speed and other processing parameters), the equilibrium curves of the reaction in non-standard state [122,123] and the experimental results (e.g., differential scanning calorimetry results). For example, in order to clarify the influence of the wettability between the reinforcements and the Al matrix on the evolution of cracks in SLM composites, the Young's contact angles (θ_Y, theoretically defined by Thomas Young) of the SLM Al_2O_3/Al−12Si couples and the SLM TiB_2/Al−12Si couples were measured (as shown in Fig. 8). It is well known that the Young's contact angle is an ideal parameter to characterize the wettability, which can be measured by the classical sessile drop technique [124,125]. By comparing Figs. 8(a) and (b), the Young's contact angle between the SLM Al−12Si alloy and TiB_2 (26°) is lower than that between the SLM Al−12Si alloy and Al_2O_3 ((79±1)°) at 1200 °C, which indicates that Al−12Si alloy exhibits a better wetting behavior with TiB_2 than with Al_2O_3. The better wettability of TiB_2/Al−12Si couples suggests that there is a higher cohesion energy (E_c) between the liquid Al−12Si and TiB_2 than that between liquid

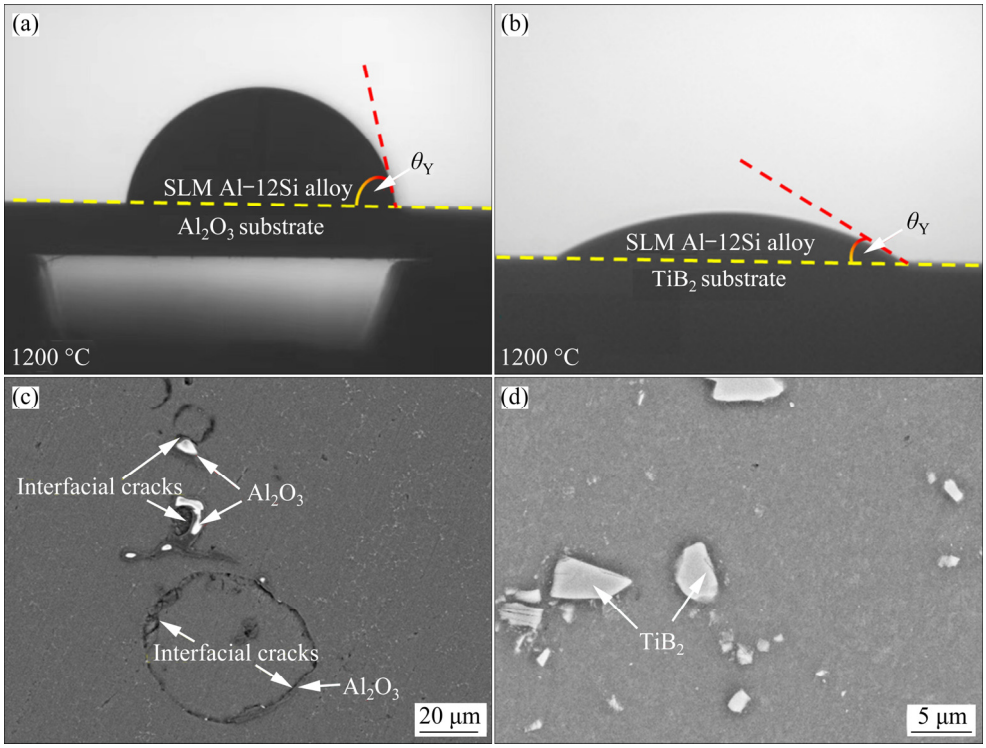

Fig. 8 Characterization of Young's contact angles for SLM Al−12Si alloy on ceramic substrate at 1200 °C (Al_2O_3 (a) and TiB_2 (Ref. [110] (b)); Morphologies of SLM Al−12Si based composites reinforced by corresponding ceramics (Al_2O_3 (c) and TiB_2 (Ref. [110] (d))

Al−12Si and Al_2O_3, implying a stronger bonding between TiB_2 particles and the Al−12Si matrix. Therefore, the weak bonding between Al_2O_3 particles and Al−12Si matrix causes SLM Al_2O_3/Al−12Si composites more sensitive to form micro-cracks at the interface between the Al matrix and Al_2O_3 particles compared with the TiB_2/Al−12Si composites, as shown in Figs. 8(c, d).

3.2 Feedstock preparation methods

Because of the important influence of the characteristics of the reinforcement on the fabrication of high-quality SLM PAMCs, as described in Section 3.1, selecting the suitable feedstock preparation methods to get the powder feedstocks with high quality is paid more attention, which can affect the heat absorption and transfer, and the distribution of the reinforcements in SLM PAMCs [117]. Table 3 lists and compares the advantages and disadvantages of the feedstock preparation methods of SLM PAMCs. Despite the tendency of the nanoparticle agglomeration, direct mixing is still a useful method, which has the advantages of the low cost and the wide applicability. But without the extra energy to force the adhesion of the reinforcement and matrix, the bonding between them is poor. The high-energy ball milling is the most common way to prepare the feedstocks. However, the high-energy during the milling changes the surface quality and the sphericity of the matrix particles, which can reduce the flowability of the feedstocks. Ultrasonic vibration dispersion is the combination of the ultrasonic vibration and mixing. Even though the agglomeration can be prevented to a certain extent, the complex processing and time consuming become the most significant disadvantage. In recent years, several smart feedstock preparation methods (i.e., electrostatic assembly, aerosol delivered adhesion, and in-situ salt-metal reaction combined with the gas-atomization) were used to prepare the powder feedstock. All these methods can get good-quality feedstock with good flowability and good adhesion. However, the complex processing, high cost and limited applicability of these methods limit the development of the SLM PAMCs with novel reinforcement and their wide application.

3.3 Effect of parameters on processing and microstructure

The in-depth and extensive work on the SLM process has indicated that, in addition to the four main parameters (i.e., the laser power (P), scanning speed (v_s), layer thickness (l_z) and hatch spacing (l_{hs})), the volumetric energy density (E_V) also has a remarkable influence on the formation of defects and microstructures of SLM alloys [33,133,134], which generally can be described by [134−136]:

$$E_V = \frac{P}{v_s l_z l_{hs}} \tag{1}$$

GU et al [137] comprehensively studied the relationship of the E_V parameter and microstructure of SLM TiC/Al−10Si−Mg composites. The field emission (FE)-SEM images revealed that the TiC

Table 3 Methods for powder feedstock of SLM PAMCs [16,19,105,126−132]

Method	Application	Advantage	Disadvantage
Direct mixing	TiB_2/Al−Cu−Mg−Si	Low cost, and wide applicability	Time consuming, and poor adhesion
High-energy ball milling	CNTs/Al−10Si−Mg, nano-SiC/AlSi7Mg and TiB_2/Al−12Si	Medium cost, wide applicability, and good adhesion	Poor flowability, and time consuming
Ultrasonic vibration dispersion	TiN/Al−10Si−Mg	Low cost, and wide applicability	Time consuming, and complex processing
Electrostatic assembly	WC/A7075, TiB_2/A7075, WC/Al−10Si−Mg and WC/A7075	Good flowability, and good adhesion	High cost, and limited applicability
Aerosol delivered adhesion	TiB_2/Al−10Si−Mg	Good flowability, and good adhesion	High cost, and complex processing
In-situ salt−metal reaction + Gas-atomization	TiC/Al, TiB_2/Al−10Si−Mg	Good flowability, and controllable size, distribution and volume fraction	High cost, complex processing, and limited applicability

particles distribute disorderly in the matrix when the volumetric energy density is low (Fig. 9(a)). With increasing the E_V, the TiC particles tend to exhibit a regular distribution and form a ring structure (Fig. 9). A similar phenomenon was also observed in SLM Al_2O_3/Al composites, which suggested that the Marangoni flow is the key factor to influence the distribution of the particles [138]. The results indicated that in the low volumetric energy density, the Marangoni convection and the attendant liquid capillary forces are too comparatively weak to force the movement of the reinforcements. Therefore, the particles are segregated randomly in the matrix [79,138]. However, with increasing the volumetric energy density, the repulsion force between the matrix and reinforcement is enhanced, which would improve the fluidity of the reinforcements in the melt pool [139]. With increasing the fluidity of the reinforcement during the SLM process, the Marangoni flow can continuously and easily stir the melt pool, thereby promoting the rearrangement rate of the reinforcements. As a result, these reinforcements accordingly tend to cluster locally around the center of the Marangoni flow pattern to form the ring, causing the pile-ups and local segregation [138]. In addition, it should be mentioned that with an excessively high volumetric energy density, the reinforcing particles can be coarsened due to the resultant grain growth of the reinforcement in the melt pool with significant thermal accumulation, as shown in Figs. 9(c, d), which can lead to the deterioration of the tensile strength and hardness.

3.4 Defect evolution

3.4.1 Defects generated from rapid solidification

As mentioned in Section 2.3, even though the addition of the reinforcements can influence the solidification behavior of the Al matrix, the formation mechanism of the defects (mainly including pores and micro-cracks) is like that of the SLM alloys. Generally, the formation mechanism of the defects during SLM process mainly refers to the balling effect [140,141], keyhole mode [142−145], conduction mode [142,146], and the lack of fusion [146,147]. For SLM Al alloys, the main formation mechanism of the defects are the keyhole mode, conduction mode, and the intermediate stage between them called transition mode [148]. QI et al [148] figured out that because the recoil pressure of the metal vapors was larger than the surface tension and the hydrostatic pressure of the liquid metal (Fig. 10(a)), the keyhole can form

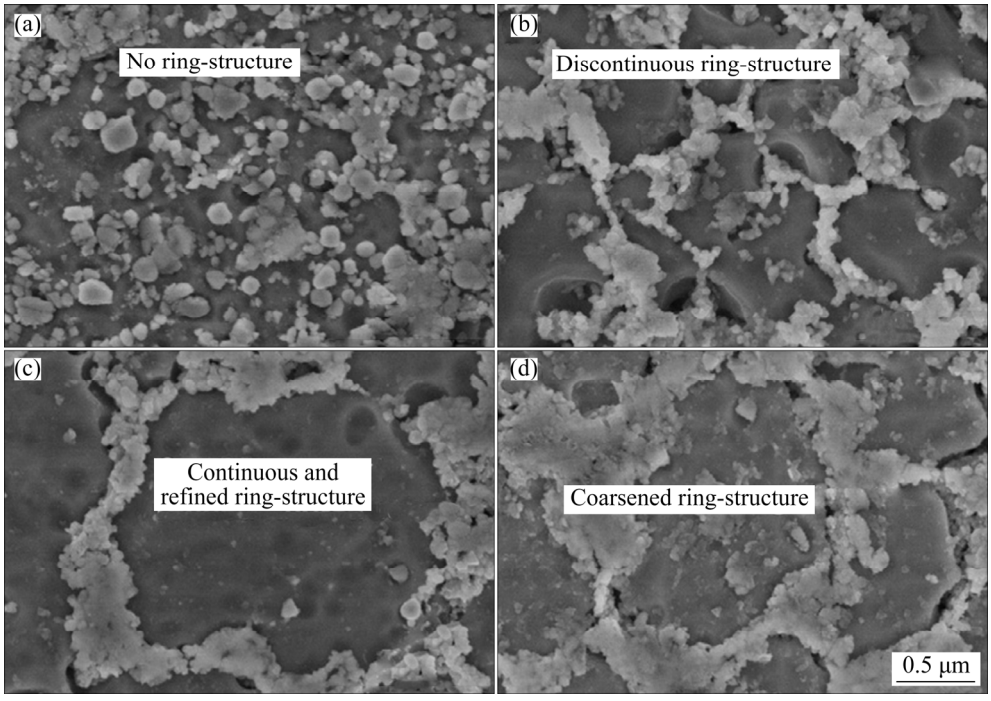

Fig. 9 High-magnification FE-SEM images showing dispersion morphologies of nanoscale TiC reinforcement in SLM-processed TiC/Al−10Si−Mg nanocomposites at different volumetric energy densities (E_V) [137]: (a) 160 J/mm^3; (b) 200 J/mm^3; (c) 240 J/mm^3; (d) 280 J/mm^3

easily when the energy density in the melt pool was sufficiently high as shown in Figs. 10(c_1, c_5)) (insets in Fig. 10(c)). With increasing the scanning speed, the volumetric energy density of the laser decreases, as depicted in Eq. (1), which is not high enough to cause the metal evaporation. Moreover, the Marangoni flow would occur from a region of the low surface tension (γ) to a region of the high surface tension according to the Heiple−Roper theory, which subsequently triggers circulation flows in the molten weld pool, as shown in Fig. 10(b) [149−151], and forms the wide and shallow melt pools, as observed in Figs. 10(c_4, c_8)) (insets in Fig. 10(c)). The high surface tension and cooling rate during SLM process with the high scanning speed can lead to the formation of the cracks in the melt pool during the solidification of the materials, which have been observed in numerous works [38,148,152]. Even though the evolution of the defects generating during the rapid solidification in SLM alloys almost has been clarified clearly by the experiments and simulations, the influence of the addition of the reinforcements on the evolution of the defects generated during the rapid solidification in SLM PAMCs has not been investigated systematically. Nowadays, the main work on the fabrication of SLM AMCs is still on the operation window of the SLM process and the optimization of the processing parameters to obtain the near-fully dense materials.

3.4.2 Defects caused by ball milling

For the fabrication of SLM PAMCs, the preparation of the powder feedstocks is the first and important step to form the near-fully dense materials. The common preparation method of the pre-powders for SLM is ball milling, which can contribute to a stable and union attachment of the particulate reinforcement and matrix powders by collisions. However, some work indicates that the collisions of the powders during ball milling can lead to the deteriorative sphericity and low flowability of the powders [79,153,154]. The powders with low sphericity and low flowability can result in the formation of defects and a low relative density of SLM alloys [31,155]. Especially, due to the low hardness of Al alloys, ball milling

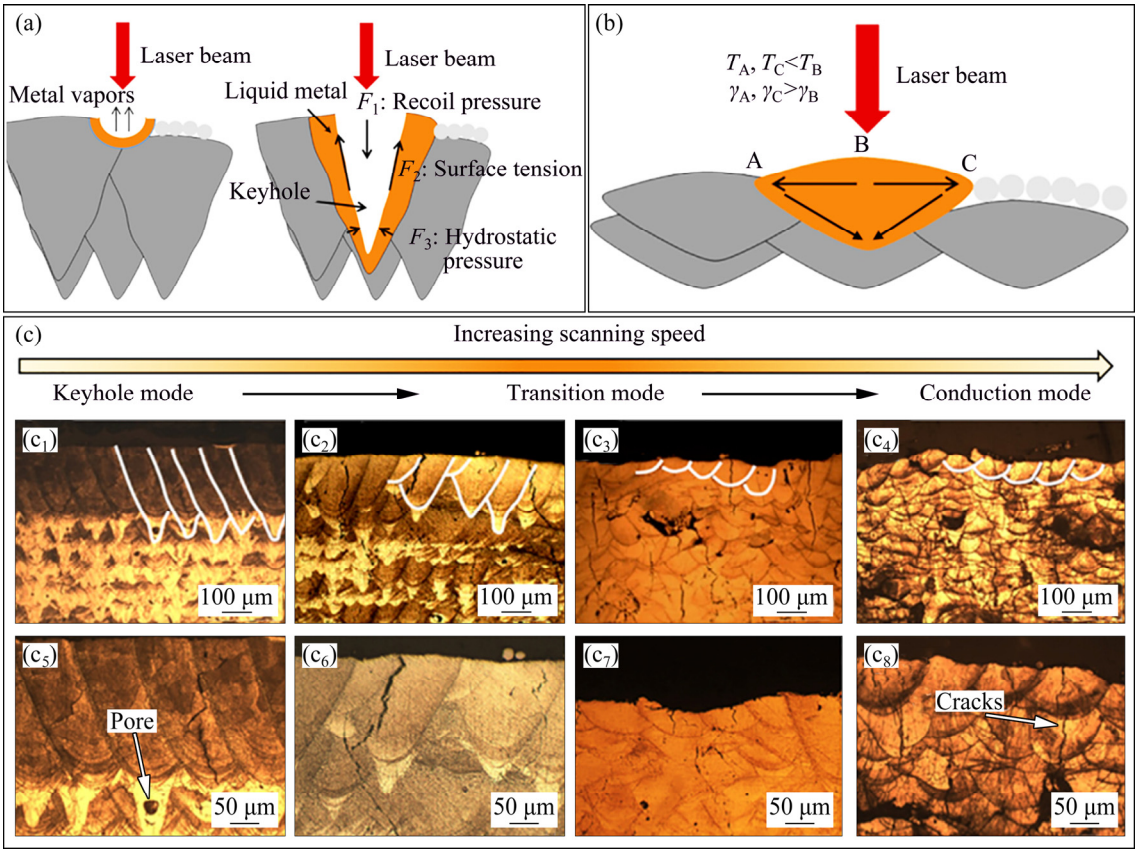

Fig. 10 Forming mechanism of defects (a), metallographic images on building direction of samples with increasing scanning speed (b), and effects of scanning speed on morphologies along building direction (c) [148]

can more easily change the surface quality and powder shape of Al matrix powders than those of other powders (i.e., Fe-based powder, Ni-based powder and Ti-based powder) [135,156,157]. In order to clarify the effect of ball milling on the preparation of Al powders for the SLM Al matrix composites, the Al−12Si powders were milled using a planetary ball mill (Retsch PM400) for different time, as shown in Fig. 11. The Al−12Si powders without ball milling have a certain agglomeration (Fig. 11(a)). After 2 h milling (the pause time is not counted), the powders with small particle size become flattened and attach around those with large size due to the collision of balls with powders (Fig. 11(b)). With increasing the milling time to 4 h (Fig. 11(c)), some spherical powders show an obviously irregular and sharp edge, and the consolidation of the powders caused by their collision is more severe. When the milling time is longer than 4 h (Figs. 11(d, e)), the quantity of irregular powders increases significantly, which is similar to the phenomenon of other powder feedstocks after long ball milling [135,157]. SURYANARAYANA [158] discussed the mechanism of ball milling comprehensively according to the numerous work. It is indicated that firstly the grinding balls run down the inside wall of the vial, which causes the friction effect of grinding balls, powders, and the vial. Secondly, the grinding balls and powders lift off and travel freely through the inner chamber of the vial, and then collide against the opposing inside wall, which causes the impact effect of the grinding balls, powders, and the vial. Due to the friction effect and impact effect during the ball milling, the force caused by the collision and friction can deform the powders and change their shape. Moreover, the energy generated during the milling tends to weld the soft powders together, which leads to the formation of the larger powders [158]. These previous works can successfully predict and explain the occurrence of the phenomena during ball milling of the powder feedstocks, as shown in Fig. 11, and are a guide to get the high quality of powder feedstocks in the future.

In order to clarify the effect of ball milling on the densification of SLM composites, the corresponding Al−12Si powders milled for different times were fabricated by SLM using the same optimized and commercial parameters supplied by SLM Solutions Group AG [32] and their morphologies are shown in Fig. 12. With increasing the milling time, the porosity of SLM Al−12Si alloy increases significantly, which indicates that long-time ball milling can cause the formation of pores in SLM Al alloys. Therefore, in order to obtain the high relative density of SLM PAMCs with fewer defects (mainly pores), the effect of ball milling on the powder feedstocks should be studied carefully or the smart preparation method of the powder feedstocks should be designed and developed to replace the ball milling method and keep the high quality of the powder feedstocks.

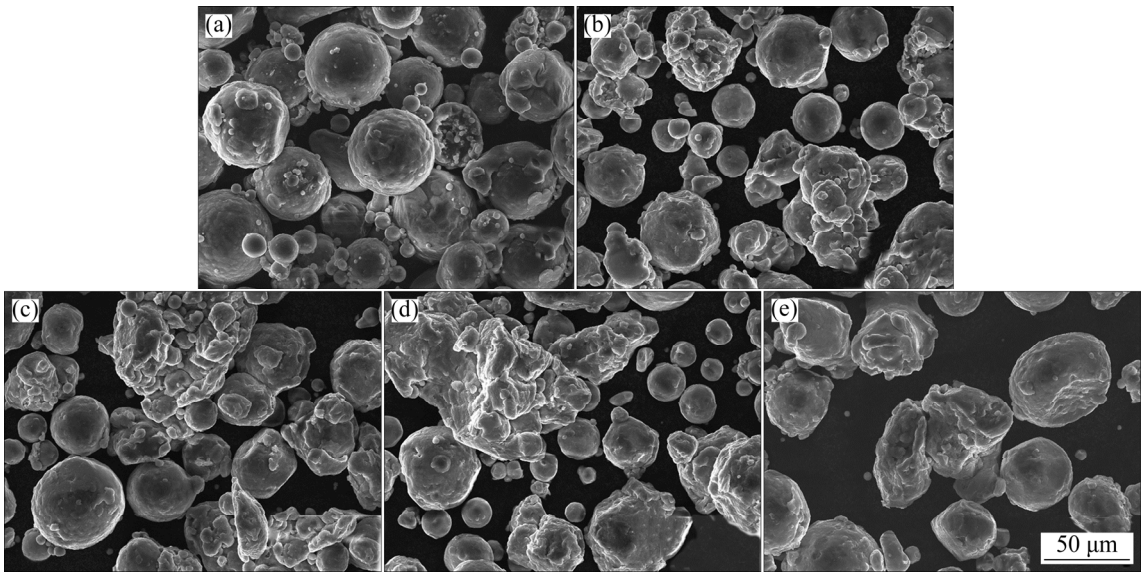

Fig. 11 Evolution of morphologies of Al−12Si powders ball-milled for different time: (a) 0 h; (b) 2 h; (c) 4 h; (d) 6 h; (e) 8 h

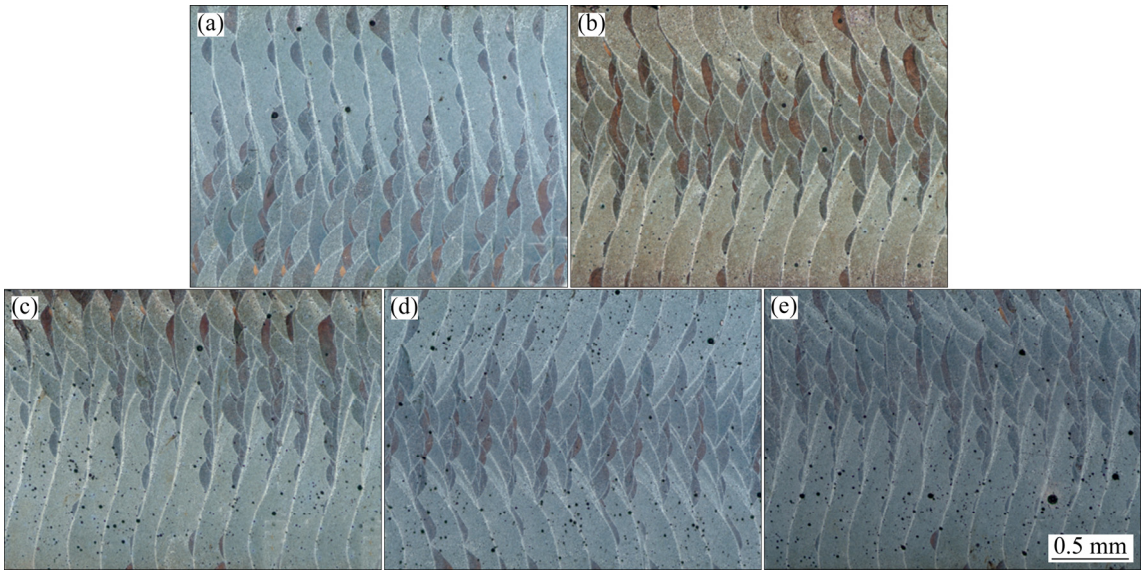

Fig. 12 Morphologies and defects of SLM Al−12Si alloys with same processing parameters but powders milled for different time: (a) 0 h; (b) 2 h; (c) 4 h; (d) 6 h; (e) 8 h

For example, LI et al [159] used the in-situ salt−metal reaction method to produce pure Al-matrix composite reinforced by nano-TiB_2 precipitates. Based on this TiB_2/CP-Al composite, nano-TiB_2/Al−10Si−Mg composite is obtained by the addition of Mg and Al−Si alloy in the next step. Finally, TiB_2/Al−10Si−Mg powders with proper composition and good quality were produced by an in-house gas-atomizer using He gas. Even though TiB_2/Al−10Si−Mg powder feedstock is complicated to obtain, the surface quality and flowability of the powder feedstock can be ensured to get the SLM nano-TiB_2/Al−10Si−Mg composite with good mechanical properties. Also, due to the nano-size TiB_2 providing numerous nuclei sites, this composite also has refined grains (~2 μm), as shown in Fig. 13(b) [159]. Except for the in-situ salt−metal reaction method, in order to obtain the powder feedstock by a simple way and to keep the good surface quality of powder feedstock, WANG et al [128] only used drum hoop mixer to combine the micro-TiB_2 particles (~3 μm) and Al−3.5Cu−1.5Mg−1Si powder together. This method can also avoid the disastrous effect of the collision between the hardened steel ball and powders on the surface quality of the powder feedstock. With these TiB_2/Al−3.5Cu−1.5Mg−1Si powder feedstock, the TiB_2/Al−3.5CuV1.5Mg−1Si composite with the evident grain refinement was fabricated successfully.

3.4.3 Defects generated from diffusion and reaction

As described in Section 2, some elements in the introduced reinforcement can diffuse in the Al matrix or react with the Al matrix due to the high temperature (>2000 K) in the melt pool achieved during SLM processing [119−121], which can cause the formation and evolution of defects in the Al matrix [61]. For example, the diffusion and reaction of Al_2O_3 in the Al matrix can lead to the formation of the pores and cracks due to the thermodynamics of Al_2O_3 phase at high temperatures. As shown in Fig. 14(a), with the optimized parameters, irregular defects are observed around the Al_2O_3 phase. LIAO et al [122] studied the equilibrium curves of the reaction of Al and Al_2O_3 in non-standard state during SLM process. Their results indicated that the main loss mechanism of Al_2O_3 is the reduction reaction of Al_2O_3 by aluminum, and Al_2O_3 loss must happen since the temperature of the melt pool is higher than the critical temperature of the reduction reaction (1793 K). As shown in Fig. 14(b), Al_2O_3 cannot evaporate directly during SLM process and the formation of Al_2O gas can change the thermophysical behavior of the Al matrix in the melt pool [122]. Therefore, in order to fabricate the near-fully dense Al matrix composites with the defects, the selection of the reinforcement of SLM Al matrix composite should also be considered carefully and the breakthrough of the forming principles should be also put forward instead of the simple parameter optimization.

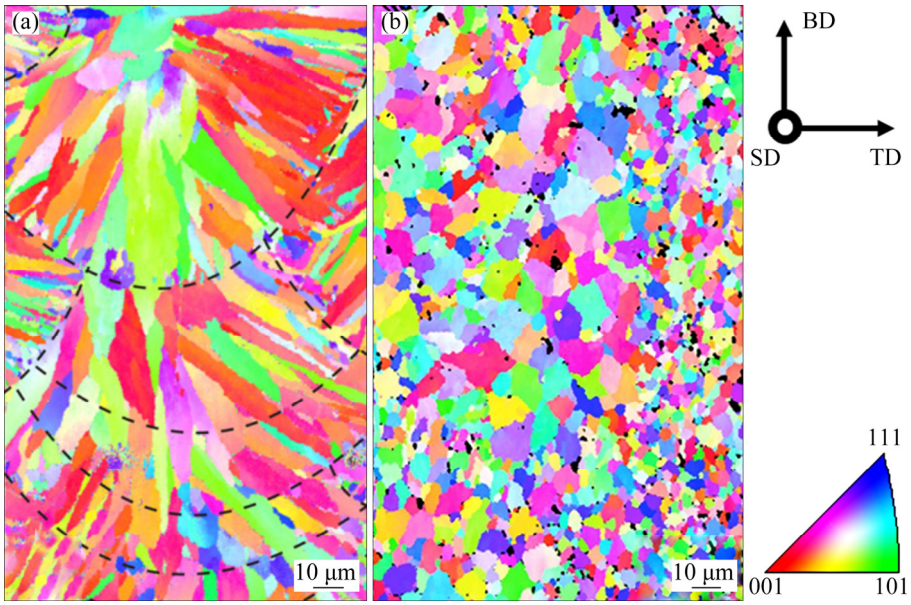

Fig. 13 EBSD orientation map and grain size distribution along building direction [72,159]: (a) SLM Al−10Si−Mg alloy; (b) SLM nano-TiB_2/Al−10Si−Mg composites of mixed salt reaction in-situ synthesis process

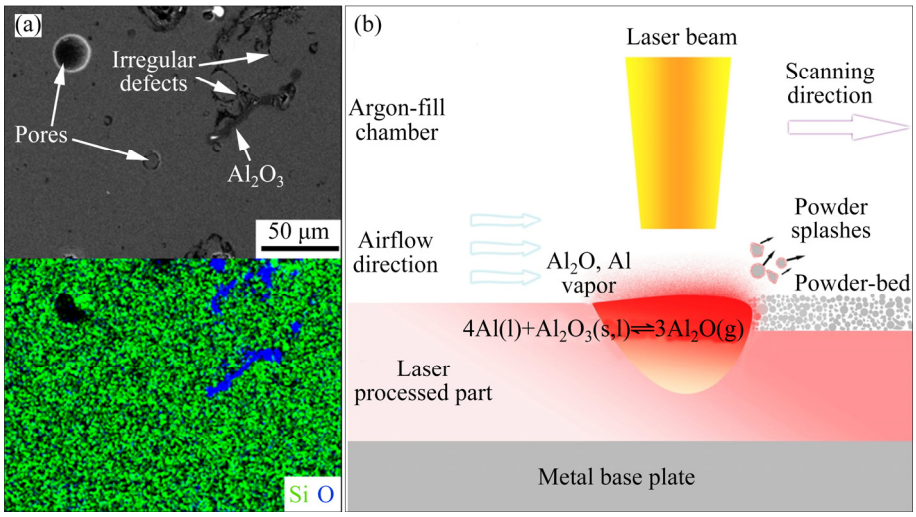

Fig. 14 SEM image and its energy-dispersive X-ray spectroscopy (EDS) map of Al_2O_3/Al−12Si composites fabricated by SLM (a), and schematic diagram of Al_2O_3 loss (b) [122]

3.5 Phase control

For most of the current SLM PAMCs, the addition of the reinforcements can lead to the formation of new phases, which can influence the chemical/physical properties significantly, especially the heat treatability. For example, even though MONTERO SISTIAGA et al [99] successfully avoid the formation and propagation of cracks along the grains of SLM Al7075 alloy according to the Si addition, the formation of other phases (e.g., Mg_2Si phase, Cu−Zn−Si−Mg phase, and Cr−Fe−Mg−Al) reduces the formation of $MgZn_2$ nano-precipitates and finally decreases the strengthening ability through heat treatment of Al7075 alloy. Therefore, it is indicated that the unpredictable reaction can change the physical/chemical properties of Al matrix and weaken the performance of SLM PAMCs, which may not meet the demand of the pre-design.

However, if the thermophysical condition of the melt pool is deeply understood, the formation of the reinforcing phase can be designed and controlled as the demand. For SiC/Al−Si composites, the Al matrix tends to react with SiC

particles depending on the temperature [160,161]:

$$4Al(l)+3SiC(s)\rightarrow A1_4C_3(s)+3Si,\quad 940\ K \le T_{temp} \le 1620\ K \tag{2}$$

$$4Al(l)+4SiC(s)\rightarrow A1_4SiC_4(s)+3Si,\quad T_{temp} \ge 1620\ K \tag{3}$$

ASTFALCK et al [162] designed and fabricated the SiC/Al−12Si composites according to Eq. (2). The reaction products are needle-like Al_4C_3 and Si phases forming between the residual SiC phase and Al matrix, as shown in Fig. 15(a). GU et al [163] also designed and developed the SiC/Al−10Si−Mg powder feedstock. According to previous work, they considered that during laser melting, the Al matrix can react with SiC phase under the specific processing conditions, when the reaction (Eq. (3)) occurs and the reaction products would be Al_4SiC_4 phase, as shown in Fig. 15(b) [160,161]. The hardness of Al_4SiC_4 phase is extremely high (around HV 1200) and is regarded as the favorable reinforcing phase for the Al matrix to improve the mechanical properties and wear resistance [164].

Moreover, according to the in-depth research of reinforcement and Al matrix [165−168], $Ti_{52.4}$-$Al_{42.2}Nb_{4.4}Mo_{0.9}B_{0.06}$(TNM)/Al−12Si composite and Al−Fe−Cr quasicrystal reinforced Al matrix composite were designed and fabricated in recent work; both exhibit enhanced mechanical properties and good wear resistance. However, it should be mentioned that due to the diffusion and reaction of the fully-melted metallic reinforcement, the unpredictable phases generated in the Al matrix [94,95] may cause the difficulty of the design and fabrication of the corresponding PAMCs.

In addition, due to the diffusion and reaction phenomena, the microstructure and the distribution of the phases display significantly non-uniform morphologies. In order to investigate the influence of such non-uniform microstructure on the properties of SLM materials, the microstructures and mechanical properties of the two kinds of SLM Al−33Cu materials fabricated from Cu/Al−4.5Cu powder mixtures and gas-atomized Al−33Cu powders, respectively, are shown in Fig. 16. As depicted in Fig. 16(a), the SLM Al−33Cu alloy from powder mixtures can achieve a compressive strength as high as that of the SLM Al−33Cu alloy of gas atomization. These results indicate that the powder mixture is a simple and suitable way to get the powder feedstocks of the SLM PAMCs with good performances. The SLM PAMCs starting from powder mixtures can also give a reference value for the development of novel SLM PAMCs starting from gas-atomized powders. However, as illustrated in Fig. 16, the SLM Al−33Cu alloy of powder mixture exhibits lower compressive strength and plastic strain ((925±39) MPa and (1.8±0.2)%, respectively) than the SLM Al−33Cu alloy of gas-atomized powders ((1197±47) MPa and (2.9±0.2)%, respectively). It is clearly suggested that the diffusion and reaction of the reinforcement and the matrix during the SLM processing can lead to the non-uniform microstructure and the formation of the weak region, which is easy to lead to the formation and propagation of the crack and the final failure of the SLM PAMCs (Figs. 16(a, b)). A similar scenario has been reported in titanium composites [145,169].

According to the above discussion, the selection of a stable reinforcement, which has less effect on the Al matrix, is important to fabricate an SLM composite, which can be pre-designed as the

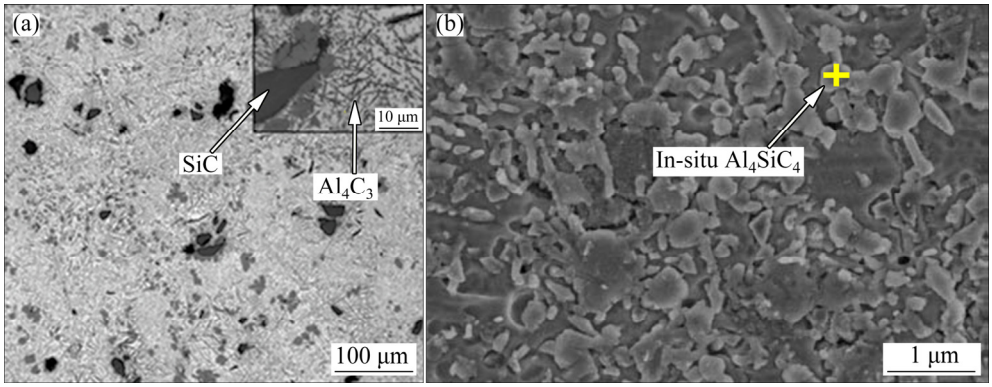

Fig. 15 SEM images of SiC/Al−Si based composites [162,163]: (a) SiC/Al−10Si−Mg; (b) SiC/Al−12Si

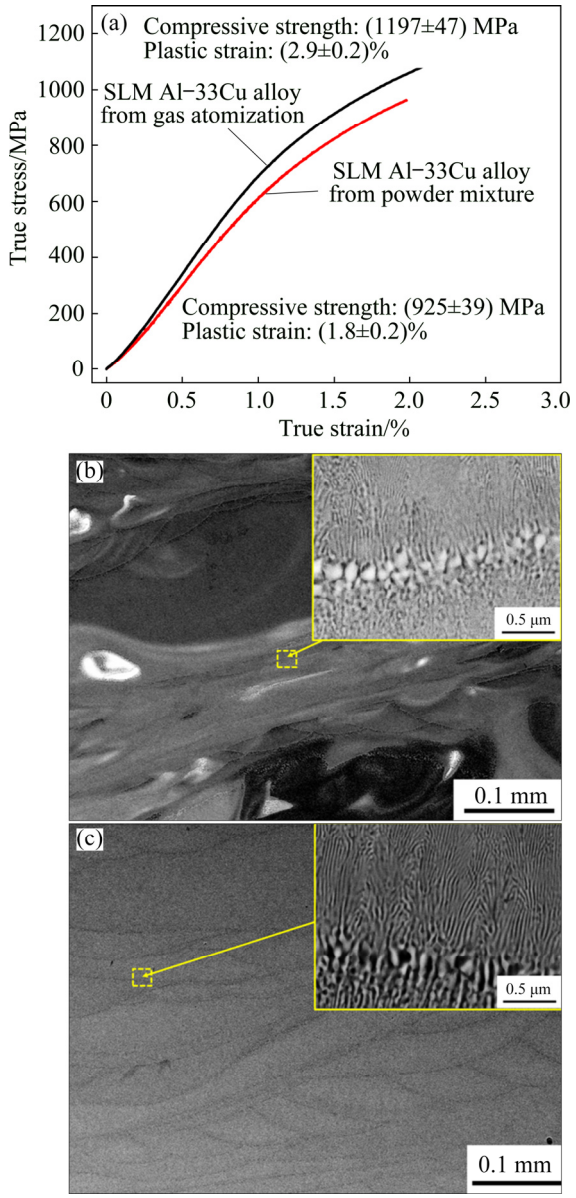

Fig. 16 Compressive true stress−strain curves of SLM Al−33Cu alloy from powder mixtures and gas atomization (a), microstructure of SLM Al−33Cu alloy from powder mixtures (b) and microstructure of SLM Al−33Cu alloy from gas atomization (c)

expected demand. TiB_2 is regarded as an ideal reinforcement in AMCs, which has a good wettability, a high chemical stability, a low solubility, and a grain refinement effect in Al matrix [170−173]. Therefore, these advantages may avoid or reduce undesirable reactions between TiB_2 and Al matrix [108,174,175]. Recently, there are several investigations about TiB_2/Al matrix composites [109,110,128]. All these SLM TiB_2/Al matrix composites exhibit refined grains and grain refinement strengthening [109,128]. Typically, two main conventional reasons may lead to the grain refinement of TiB_2/Al matrix composites. 1) Under suitable conditions, the TiB_2 particles can react with the Al matrix and a nano-sized $TiAl_3$ interface with a few atomic layers may form between the TiB_2 particles and the Al matrix [100,174,176], which can provide more nuclei for crystal growth than the matrix alloy, thereby eventually promoting a significant grain refinement. However, this effect depends on not only the reaction condition but also the activity of the TiB_2 phase [174]. 2) Due to a preferable natural stacking sequence of Al atoms on TiB_2 [106], fine TiB_2 particles can also refine the grains of the Al alloys directly. Thus, distinct grain refinement of the Al matrix but no evident reaction interface between TiB_2 and Al alloys are observed [106,177]. According to the analyses of the composition and crystal structure of the phases by transmission electron microscopy (TEM) and its corresponding EDS, there is no evident reaction between TiB_2 and Al matrix or diffusion of Ti and B into Al matrix (Fig. 17) [110,128]. Moreover, the important result is that the heat-treatable Al matrix still has a strong precipitation-hardening ability after the commercial T6 heat treatment, which suggests that the addition of TiB_2 does not significantly affect the heat treatability of Al matrix [128]. Until now, compared with TiB_2, most of the reinforcement in SLM PAMCs would change the heat treatability of the Al matrix because of the reaction and diffusion during SLM processing. All results about SLM TiB_2/Al matrix composites indicate that TiB_2 can not only cause load-bearing strengthening and grain refinement strengthening of Al matrix but also maintain the physical/chemical properties of the Al matrix, which implies that the TiB_2 is an ideal reinforcement for the fabrication of the high-strength SLM PAMCs with the high relative density.

4 Performance of current PAMCs

Current researches about the SLM PAMC mainly have been focused on the mechanical properties (i.e., strength, plastic strain and hardness) and wear resistance due to the application background of PAMCs in the industry, as shown in Table 2, and all corresponding properties are summarized in Table 4. The statistics in Table 4 refer to the current SLM Al matrix composites

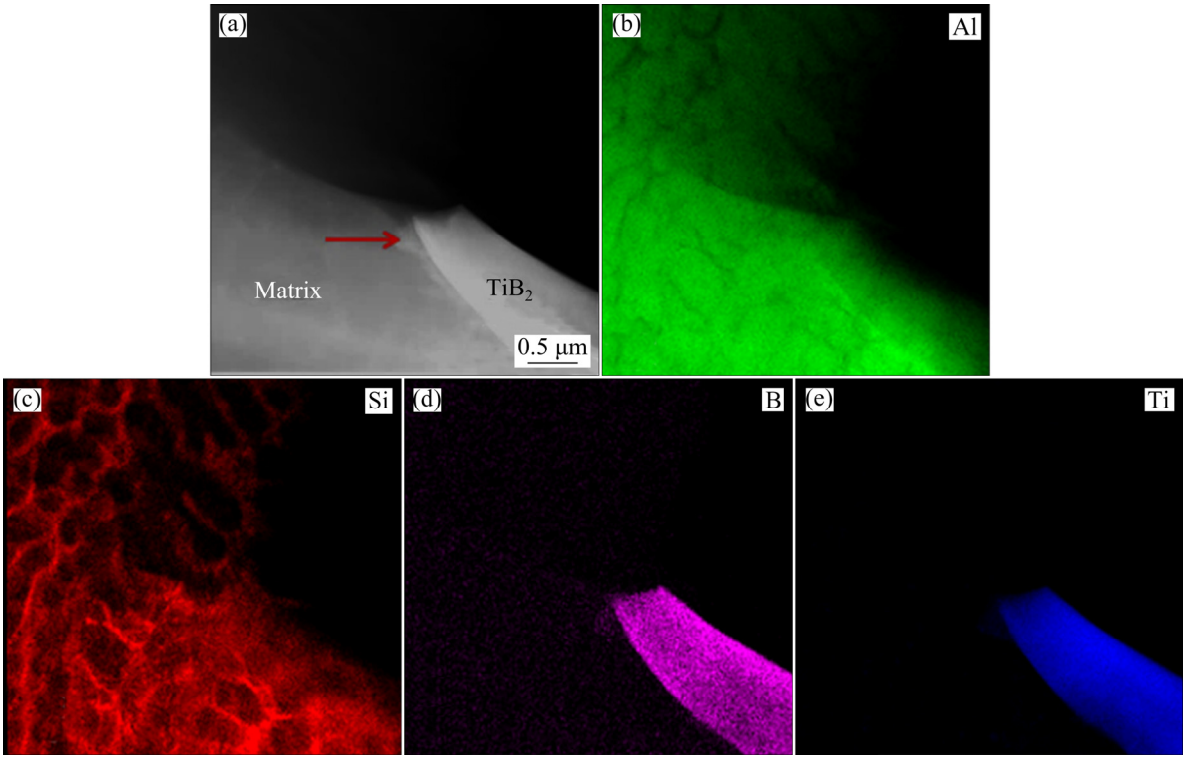

Fig. 17 Bright-field TEM image (a) and corresponding EDS maps (b−e) obtained near interface for SLM TiB_2/Al−12Si composite [110]

according to different series Al matrix (CP-Al, Al−Si alloys, Al−Cu−Mg−Si alloys and Al−Zn alloys) and the different reinforcement including metallics (i.e., Al−Fe−Cr quasicrystal and TNM), and ceramics (i.e., Fe_2O_3, Al_2O_3, TiC, SiC, AlN, TiB_2 and carbon nanotubes). In this work, the discussion is based on the categories of the Al matrix involving the heat-treatable and non-heat-treatable Al alloys. Even though the addition of some reinforcements in the Al matrix can cause the formation of defects, most of these reinforcements can improve the mechanical properties and wear resistance of SLM Al alloys dramatically [137,193].

4.1 SLM CP-Al matrix composites

As the most common matrix of the conventional PAMCs [194], CP-Al powder was firstly used as the matrix for the fabrication of SLM Al matrix composites [180]. DADBAKHSH et al [178−181] successfully fabricated the 15wt.%Fe_2O_3/CP-Al composites by SLM, which exhibit a higher microhardness than the SLM CP-Al. However, even though the SLM 15wt.%Fe_2O_3/CP-Al composite has enhanced mechanical properties, this composite has a low relative density (~70%). The in-depth studies indicated that during laser melting, the reaction between the Al matrix and Fe_2O_3 tends to occur at the interfaces of two phases, which results in the formation of Fe_3Al, Al_2O_3 and extra heat. The formation of the new phase and the extra heat can influence the fluidity and stability of the melt pool, which is detrimental to the density of the composites [181]. In addition to Fe_2O_3 particles, Al_2O_3 particles were also selected as the reinforcement of CP-Al based composites to improve the mechanical properties and enhance the macroscale wear behavior [138]. It was indicated that the fitting scanning speed can improve the relative density (97%), microhardness ($HV_{0.1}$ 175) and wear resistance (i.e., low coefficient of friction (0.11) and low wear rate (4.75×10^{-5} $mm^3\cdot N^{-1}\cdot m^{-1}$)) simultaneously [123,138, 183]. However, due to the reaction of Al and Al_2O_3 during the laser melting, the densification of SLM 20wt.%Al_2O_3/CP-Al composite was difficult to further improve. An exciting work reported by HAN et al [123,182] indicates that the SLM 4vol.%Al_2O_3/CP-Al composites can have a high relative density (99%) and enhanced performances. According to the measurement of surface quality of

Table 4 Mechanical properties of SLM PAMCs

Composite	ρ_R/%	Reinforcing phase	Strength/ MPa	Hardness	Wear resistance	Ref.
15wt.%Fe_2O_3/CP-Al	~70	Fe_2O_3, $FeAl_2O_4$, $Al_{13}Fe_4$ and Al_2O_3	−	$HV_{0.1}$ ~80	−	[178−181]
20wt.% Al_2O_3/CP-Al	81−97	Al_2O_3	−	$HV_{0.1}$ 148−175	*	[138]
4vol.%Al_2O_3/CP-Al	~99	Al_2O_3	σ_s= 100−160	$HV_{0.1}$ ~48	*	[123,182]
30wt.%Al−Fe−Cr (QC)/CP-Al	~99	Al_2Cu, (Al−Cu−Fe−Cr(QC) or Al−Fe−Cr(QC))	σ_s=292	$HV_{0.2}$ 240−260	*	[95,183]
30vol.%TiC/Al	~99	TiC	C_y=800	−	−	[129]
15wt.%Fe_2O_3/ Al−10Si−Mg	~80	$Al_{13}Fe_4$, Al_2O_3, Al_3FeSi_2, $Al_{0.7}Fe_3Si_{0.3}$ and $Al_{0.5}Fe_3Si_{0.5}$	−	$HV_{0.1}$ ~165	−	[180]
5wt.%TiC/Al−10Si−Mg	~99	TiC	σ_s= 400−486	$HV_{0.2}$ 159−181	*	[137,184,185]
20wt.%SiC/Al−10Si−Mg	95−97	Al_4SiC_4 and SiC	−	$HV_{0.1}$ 110−214	*	[163,186]
15wt.%Al_2O_3/ Al−10Si−Mg	87−99	Al_2O and Al_2O_3	−	−	*	[122,187]
7vol.%TiB_2/ Al−10Si−Mg	~99	TiB_2	σ_s= 530±16	$HV_{0.3}$ 191±4	−	[159]
3.4vol.%TiB_2/Al−10Si−Mg	~99	TiB_2	σ_s= 522−530	−	−	[105]
2wt.%AlN/Al−10Si−Mg	~97	AlN	−	$HV_{0.05}$ 79−85	*	[92,188,189]
1wt.%CNTs/Al−10Si−Mg	~95	CNTs and some Al_4C_3	σ_s≈499	HV 143±6	−	[190,191]
2wt.%TiN/Al−10Si−Mg		TiN	−	$HV_{0.1}$ 145±45	*	[130,131]
0.5wt.%CNTs/ Al−10Si−Mg	~99	CNTs and some Al_4C_3	σ_s≈420	154	*	[126]
20vol.%TNM/Al−12Si	~99	$AlTi_3$, Al_6MoTi and MoNb	C_y= (420±4)	−	*	[94]
10vol.%SiC/Al−12Si	~97	SiC, Si and Al_4C_3	−	−	*	[162]
2wt.%TiB_2/Al−12Si	~99	TiB_2	C_y= (225±4)	$HV_{0.05}$ 142±6	−	[109,110]
5wt.%TiC/Al−15Si	~97	TiC	−	HV_1 ~173	*	[192]
5vol.%TiB_2/ Al−Cu−Mg−Si	~99	TiB_2	C_y= (191±12)	$HV_{0.05}$ 142±7	−	[128]
5vol.%TiB_2/ Al−Cu−Mg−Si (T6)	~99	TiB_2	C_y= (401±9)	$HV_{0.05}$ 187±6	−	[128]
1vol.%ZrH_2/A7075 (T6)	~99	Al_3Zr	σ_s≈417	−	−	[19]

ρ_R: Relative density; C_y: Compressive yield strength; *: Improvement

this composite by atomic force microscopy (AFM), irregular nano-sized pores are present around the nano-Al_2O_3 particulates (50 nm). It is indicated that the nano-size of the reinforcement can reduce the influence of the reaction between Al_2O_3 and Al on the formation of the pores, which can lead to the decreasing porosity of the SLM Al_2O_3/CP-Al composites.

4.2 SLM Al−Si matrix composites

Due to the good castability and weldability of Al−Si alloys during laser processing, Al−Si alloys have been the first candidate fabricated by SLM, and SLM Al−Si alloys have a more outstanding performance than the Al−Si alloys fabricated by the conventional method [195−197]. Therefore, SLM Al−Si matrix composites were fabricated and

characterized in early stages. Until now, SLM Al−Si matrix composites are the most widely designed and studied in the SLM Al matrix composites, and their reinforcements include ceramics like SiC, Al_2O_3 and TiC, and the metallics like TNM and Al−Fe−Cr quasicrystal. For Al−Si matrix composites, the matrix is mainly Al−12Si, Al−15Si or Al−10Si−Mg, which has a high Si content. For Al−10Si−Mg alloy, even though there is a formation of Mg_2Si after the heat treatment, the precipitation hardening from Mg_2Si is not strong. The reason is that the formation of the nano-scale eutectic Si can cause strong Orowan strengthening, which weakens the effect of precipitation hardening from Mg_2Si [198−200]. Therefore, in the present work, SLM Al−10Si−Mg based composites were put together with Al−12Si and Al−15Si into the discussion. It is well known that Al−Si series alloys are used as structural materials for engine blocks and pistons due to their high wear resistance and high specific strength [201,202]. The current studies are about the further improvement of the mechanical properties and the wear resistance of SLM Al−Si matrix. According to Table 3, all results indicate that the addition of reinforcement can improve the micro-hardness and wear resistance of SLM PAMCs compared to the corresponding SLM alloy. However, high volume fraction reinforcements in SLM PAMCs may cause the formation of the pores and reduce the mechanical properties. As shown in Table 4, the SLM PAMCs with higher volume/mass fraction of reinforcement have a higher strength, hardness and wear resistance, which has a similar changing trend as the evolution of the fraction−properties relationship of the conventional composites [203]. However, the volume/mass fraction of the reinforcements can influence the optimized parameters of the near-fully dense composites, which finally results in the variation of the properties and the microstructure of SLM composites. Therefore, the relationship among the fraction, processing parameter, densification and properties of the SLM composites should be studied further.

In addition, some novel SLM metallic/Al−Si matrix composites were designed and fabricated successfully. For these composites, the Al matrix would react with the reinforcement significantly, but their properties are improved more dramatically than SLM ceramic/Al−Si matrix composites. Therefore, through the reasonable design of these composites, this kind of composites can obtain outstanding properties and have an apparent advantage of the applications [50].

4.3 SLM Al−Cu matrix composites

Due to their high specific strength, excellent fatigue properties and good damage tolerance, Al−Cu alloys are widely used in the aerospace industry [204,205]. However, due to the limitation of the research and development of SLM technology, near-fully dense Al−Cu alloys are difficult to be produced and very rare work about SLM Al−Cu matrix composites was reported in recent years [37,38,206,207]. Based on the successful fabrication of the SLM Al−Cu alloys, the theory and experience for the formation of the SLM Al−Cu alloy were used to produce the SLM Al−Cu based composites by WANG et al [128]. Because the Al−Cu alloys are mainly used as the construction materials, the main goal of the design of SLM Al−Cu based composites is to improve the mechanical properties of the Al−Cu matrix further. Based on this design concept, WANG et al [128] designed and fabricated SLM TiB_2/Al−3.5Cu−1.5Mg−1Si with higher compressive strength ((191±12) MPa) than SLM Al−3.5Cu−1.5Mg−1Si alloy ((157±6) MPa). Their results indicated that the addition of TiB_2 can refine the grains of the Al matrix and enhance the compressive strength of the Al−Cu−Mg−Si alloy through grain boundary strengthening. It is striking that the addition of TiB_2 cannot change the heat treatability of the Al matrix even though the refined grains are almost retained. Therefore, after T6 heat treatment, the compressive strength of TiB_2/Al−3.5Cu−1.5Mg−1Si is further increased to (401±9) MPa, which is still higher than that of SLM Al−3.5Cu−1.5Mg−1Si alloy under the T6 heat treatment condition.

5 Prospective viewpoints

Based on the above discussion, the future issues for SLM Al matrix composites mainly involve five aspects: (1) Pre-design of SLM PAMCs; (2) How to produce the high-quality powder feedstock of SLM PAMCs by the greater, faster, better and more economical preparation method; (3) Innovative forming theory of SLM PAMCs; (4) Fracture mechanism of SLM PAMCs;

(5) More investigations on other chemical/physical properties (such as fatigue and high-temperature strength, wear resistance, conductivity, and corrosion).

5.1 Pre-design of constituent of SLM PAMCs

For aluminum matrix composites, the design of their constituent is key factor to determine their properties, mainly referring to the properties of the matrix and reinforcement, the proportion of the matrix and reinforcement, the distribution of the reinforcement in the matrix, and the shape of the reinforcement [208,209]. However, due to the special solidification behavior described in Section 2, there are particular thermophysical phenomena during laser melting (as shown in Fig. 4), which is different from the conventional method like stir casting, vacuum casting, squeeze casting, hot or cold compaction [56,110,210]. For the PAMCs manufactured by the conventional methods, the proportion of the matrix and reinforcement, and the shape of reinforcement are easy to control by temperature and pressure, and conventional PAMCs is convenient to design and fabricate [54]. From this aspect, the design and fabrication of SLM PAMCs as the demand still encounter many obstacles due to the reaction and diffusion of the matrix and reinforcement during the laser melting, which is difficult to control, as mentioned in Section 3.3.

Even though there are some obstacles, the advantages of the high-performance and complex geometries of SLM PAMCs still attract extensive research attentions. The one important reason is that most SLM Al matrix alloys can exhibit high strength and wear resistance due to the formation of the non-equilibrium phases and fine microstructures caused by the high cooling rate (10^4−10^5 K/s) [75]. It can promise that Al matrix composites can have a high-performance matrix. Therefore, in order to obtain more high-performance SLM PAMCs, the novel SLM Al alloys should be developed and investigated in the future. Recently, Al−Mg−Sc alloy (known as Scalmalloy®: high strength, high ductility, and high corrosion resistance) has been fabricated by SLM successfully, which has much higher strength than the wrought Al−Zn alloys [26,211]. Furthermore, due to the high strength and the wide application in the aerospace construction, the fabrication of the near-fully dense SLM Al−Zn alloy and their composites is the current hot topic. However, the cracks caused by the hot-tear along the grains are the main problem, which still cannot be solved effectively so far.

Moreover, the selection of the reinforcements is also the key factor, which would influence the formation of the reinforcing phase, the evolution of the grains and defects, and the final properties of the composites, as mentioned in Section 3.1. Therefore, the in-depth understanding of the solidification behavior, the physical properties of the reinforcing phases (such as coefficient of expansion, wetting behavior and melting point) and other thermophysical characteristics in the melt pool should be considered carefully to design and control the microstructure and properties of SLM PAMCs. As listed in Table 4, the reinforcements like TiB_2, carbon nanotubes (CNTs), TiC, and AlN have less reaction with the Al matrix, which are easy to be used to manipulate the microstructure and properties of their Al matrix by the design of the volume fraction of the reinforcement. Therefore, these kinds of SLM PAMCs are progressive thinking to avoid the disastrous reaction and diffusion between the Al matrix and the reinforcements during SLM process, and to reduce their influence on the microstructure design.

Except for the reasonable selection of the reinforcement and matrix, the volume/mass fraction of these constituents in PAMCs is also important to design the properties of PAMCs, However, until now, the current highest volume fraction of the reinforcement for SLM PAMCs is 20%, which is lower than that (20−40 vol.%) of the conventional PAMCs [209,212]. A considerable number of works indicate that the load-bearing strengthening of the PAMCs with the low content of reinforcements (<20 vol.%) is low and cannot improve the strength significantly compared with the conventional Al matrix composites [212−215]. Therefore, the next hot topic for the fabrication of SLM PAMCs would be the SLM PAMCs with a high-volume fraction of the reinforcement to further improve the strength of SLM PAMCs.

In addition, the in-depth understanding of the wetting behavior and interfacial interaction of the reinforcement and the matrix is also the primary issue for the interfacial quality and the thermodynamic stability of PAMCs, which affects not only the densification of the PAMCs but also their strength [108,110]. Moreover, the research of

the wetting behavior and interfacial bonding can also contribute to the clarification of the principle problems during the laser melting such as the grain refinement, the reaction between the matrix and the reinforcement, diffusion mechanism and the thermal stability of the microstructure. The investigations on these issues are helpful to the pre-design of the constituents of SLM PAMCs.

5.2 Preparation of powder feedstock of SLM PAMCs

As shown in Section 3.4.2, the quality of the powder feedstock is important to fabricate the near-fully dense SLM PAMCs with high performance. Due to the simple operation, reproducible results by the energy and speed control, and the wide range of materials [153,158], ball milling was the first and common choice to prepare the powder feedstock of SLM PAMCs. However, even though reducing the milling time can relieve the effect of the long-time collision on the surface quality, this effect cannot be completely avoided. The reduced quality of powder feedstocks can significantly deteriorate the density and performance of SLM PAMCs. Therefore, to find the advanced mixing method, which cannot affect the surface quality of powders, is pivotal for the improvement of the densification and the performance of SLM PAMCs. In recent years, some smart methods are put forward and the powder feedstocks fabricated by these smart methods show a good combination of the reinforcement and the matrix. They are also good for the uniform distribution of the reinforcement around/in the matrix [19,216]. Firstly, the nanoparticle assembly method is used to produce a metal powder with the nanoparticle. This method can introduce equiaxed grain growth and reduce hot tearing. However, the volume fraction of the nanoparticles is still not as high as that of the conventional composites (>20 vol.%) [212−215]. Accordingly, the strength of the composites may not be significantly enhanced. Secondly, the in-situ synthesis method is used to produce the TiB_2/Al−10Si−Mg composite, which can lead to the homogeneous distribution of the reinforcement, the refined grains of the Al matrix, and the improvement of the Al matrix. By this method, the Al powder feedstocks reinforced by the high-volume fraction of reinforcements used for SLM PAMCs can be fabricated [217,218] to improve strength further. However, only some special reinforcements (i.e., TiB_2, TiC, Mg_2Si and Al_2O_3) can be fabricated by this method [219], which limits the broad applications of this method on the fabrication of the powder feedstocks for SLM PAMCs. Therefore, in the next few years, developing a new novel and universal method to produce the powder feedstocks for SLM PAMCs is a significantly important part to fabricate the SLM PAMCs with high performance.

5.3 Theoretical breakthrough of forming mechanism of SLM PAMCs

Understanding the forming mechanism is the most important step to fabricate the near-fully dense materials with high performance [71]. As discussed in Section 2.3 and Section 3.2.1, the densification of some SLM PAMCs is still a major problem, mainly due to the formation of the pores and cracks. However, grain refinement caused by the addition of the second phase is a good way to reduce the hot-tear cracks among grains of matrix alloys, which is a big theoretical breakthrough of the forming mechanism of SLM PAMCs in recent years [19]. Even though this discovery is important and useful, it cannot solve all problems about the formation of cracks and pores in SLM alloys [220,221]. It is indicated that this theoretical breakthrough is a limited method. Therefore, in future work, the new forming mechanism of SLM PAMCs is urgent to be built to avoid the formation of defects. Furthermore, the addition of the reinforcement can also affect solidification behavior during the SLM process, which would increase the difficulty of the understanding of the forming mechanism of SLM PAMCs. So far, it seems that TiB_2 can not only refine the grains of the Al matrix but also have no evident detrimental effect on the Al matrix. Therefore, TiB_2 is considered as a good reinforcement in Al matrix composites and should be studied further in the future.

5.4 Strengthening and fracture mechanism of SLM PAMCs

Until now, the research on the SLM PAMCs is still about the over-simplified measurement and characterization of mechanical properties. The comprehensive work has not been carried out to clarify the fracture mechanism of SLM PAMCs. The relationship of the microstructure, the

strengthening/toughening mechanism, and the fracture mechanism of SLM PAMCs is still not explored clearly. Based on the current progress, many researchers have individually investigated the strengthening mechanism of the SLM TiB_2/Al matrix composites, which indicates that the grain refinement strengthening, load-bearing strengthening and Orowan strengthening can synergistically enhance the Al matrix and the corresponding composites demonstrate an improved strength and larger plasticity [110,128,159]. However, besides the classical mechanism, the SLM PAMCs exhibit a unique microstructure of SLM materials due to the special solidification behavior and formation mode of SLM PAMCs. For example, because of the layer-by-layer forming mode in SLM process, SLM PAMCs have a layer-by-layer mesoscale feature resulting in the change of crack path during propagation [222]. The change of the crack propagation during the failure can affect mechanical properties such as fracture toughness, fatigue strength, tensile/compressive strength and plasticity. Therefore, for SLM PAMCs, the existence of the hard reinforcement and the meso-structure can synergistically affect the strengthening and fracture mechanism. To summarize, the extensive understanding of the strengthening and fracture mechanism fracture would be an important step to design the high-strength SLM PAMCs and bring SLM PAMCs into the industrial market.

5.5 Investigation on more chemical/physical properties of SLM PAMCs

For the SLM Al alloys, besides the mechanical properties, the coefficient of thermal expansion, corrosion-resistance, fatigue, and wear resistance of SLM were also investigated. The investigations of these works indicate that SLM Al alloys have higher corrosion resistance, fatigue resistance and wear resistance, and a lower coefficient of thermal expansion because of the higher hardness and refined secondary phases [195,196,201,222−224]. This implies that these properties of SLM PAMCs may also be enhanced due to the improvement of the Al matrix. The results on the improvement of wear resistance of SLM PAMCs can support this conclusion [192,225]. Furthermore, the addition of the hard-particulate reinforcements can improve the wear resistance further [192,225]. However, until now, there are still few reports about the corrosion resistance, fatigue resistance and coefficient of thermal expansion of SLM PAMCs, which is difficult to confirm the corresponding interaction effect of Al matrix and reinforcements on these properties. For the properties of SLM PAMCs at high temperatures, they are also rarely investigated. However, due to the coarsening phenomenon of the secondary phase with increasing temperature, the strength of SLM Al−10Si−Mg drops off dramatically and the plasticity increases significantly [226], which implies that the SLM PAMCs may suffer the same condition. But whether the addition of the hard-particulate reinforcements can weaken this phenomenon is difficult to conclude.

Therefore, in the future, there are many important investigations on other chemical/physical properties (fatigue and high-temperature strength, wear resistance, conductivity, corrosion, etc) needed to be done, which is not only helpful to the inner relationship of the Al matrix and the reinforcements of SLM PAMCs but also the key to the application of SLM PAMCs.

Acknowledgments

The authors would like to thank Prof. T. NIENDORF, Prof. X. LIN, Prof. S. PAULY, and Prof. L. C. ZHANG for the technical assistance and insightful discussion.

References

[1] CHEN Zhang-wei, LI Zi-yong, LI Jun-jie, LIU Cheng-bo, LAO Chang-shi, FU Yue-long, LIU Chang-yong, LI Yang, WANG Pei, HE Yi. 3D printing of ceramics: A review [J]. Journal of the European Ceramic Society, 2019, 39(4): 661−687.

[2] NGO T D, KASHANI A, IMBALZANO G, NGUYEN K T Q, HUI D. Additive manufacturing (3D printing): A review of materials, methods, applications and challenges [J]. Composites Part B: Engineering, 2018, 143: 172−196.

[3] LIANG Shun-xing, WANG Xue-qing, ZHANG Wen-chang, LIU Yu-jing, WANG Wei-min, ZHANG Lai-chang. Selective laser melting manufactured porous Fe-based metallic glass matrix composite with remarkable catalytic activity and reusability [J]. Applied Materials Today, 2020, 19: 100543.

[4] ZHANG Lai-chang, LIU Yu-jing, LI Shu-jun, HAO Yu-lin. Additive manufacturing of titanium alloys by electron beam melting: A review [J]. Advanced Engineering Materials, 2018, 20(5): 1700842.

[5] EMELOGU A, MARUFUZZAMAN M, THOMPSON S M,

SHAMSAEI N, BIAN L. Additive manufacturing of biomedical implants: A feasibility assessment via supply-chain cost analysis [J]. Additive Manufacturing, 2016, 11: 97−113.

[6] THOMPSON M K, MORONI G, VANEKER T, FADEL G, CAMPBELL R I, GIBSON I, BERNARD A, SCHULZ J, GRAF P, AHUJA B, MARTINA F. Design for additive manufacturing: Trends, opportunities, considerations, and constraints [J]. CIRP Annals−Manufacturing Technology, 2016, 65(2): 737−760.

[7] PITICESCU R, KATZ-DEMYANETZ A, POPOV V V, KOVALEVSKY A, SAFRANCHIK D, KOPTYUG A, VLAICU I. Powder-bed additive manufacturing for aerospace application: Techniques, metallic and metal/ceramic composite materials and trends [J]. Manufacturing Review, 2019, 6: 1−13.

[8] LI Neng, HUANG Shuai, ZHANG Guo-dong, QIN Ren-yao, LIU Wei, XIONG Hua-ping, SHI Gong-qi, BLACKBURN J. Progress in additive manufacturing on new materials: A review [J]. Journal of Materials Science & Technology, 2019, 35(2): 242−269.

[9] ZHANG Lai-chang, ATTAR H. Selective laser melting of titanium alloys and titanium matrix composites for biomedical applications: A review [J]. Advanced Engineering Materials, 2016, 18(4): 463−475.

[10] LIU Y J, ZHANG Y S, ZHANG L C. Transformation-induced plasticity and high strength in beta titanium alloy manufactured by selective laser melting [J]. Materialia, 2019, 6: 100299.

[11] LOEBER L, FLACHE C, PETTERS R, KUEHN U, ECKERT J. Comparison of different post processing technologies for SLM generated 316l steel parts [J]. Rapid Prototyping Journal, 2013, 19(3): 173−179.

[12] DADBAKHSH S, MERTENS R, HAO Liang, van HUMBEECK J, KRUTH J P. Selective laser melting to manufacture “in situ” metal matrix composites: A review [J]. Advanced Engineering Materials, 2019, 21(3): 1801244.

[13] ZHANG L C, KLEMM D, ECKERT J, HAO Y L, SERCOMBE T B. Manufacture by selective laser melting and mechanical behavior of a biomedical Ti−24Nb−4Zr−8Sn alloy [J]. Scripta Materialia, 2011, 65(1): 21−24.

[14] COSTA M M, DANTAS T A, BARTOLOMEU F, ALVES N, SILVA F S, MIRANDA G, TOPTAN F. Corrosion behaviour of PEEK or β-TCP-impregnated Ti6Al4V SLM structures targeting biomedical applications [J]. Transactions of Nonferrous Metals Society of China, 2019, 29(12): 2523−2533.

[15] MURR L E, GAYTAN S M, RAMIREZ D A, MARTINEZ E, HERNANDEZ J, AMATO K N, SHINDO P W, MEDINA F R, WICKER R B. Metal fabrication by additive manufacturing using laser and electron beam melting technologies [J]. Journal of Materials Science & Technology, 2012, 28(1): 1−14.

[16] YU W H, SING S L, CHUA C K, KUO C N, TIAN X L. Particle-reinforced metal matrix nanocomposites fabricated by selective laser melting: A state of the art review [J]. Progress in Materials Science, 2019, 104: 330−379.

[17] BARTOLOMEU F, BUCIUMEANU M, PINTO E, ALVES N, SILVA F S, CARVALHO O, MIRANDA G. Wear behavior of Ti6Al4V biomedical alloys processed by selective laser melting, hot pressing and conventional casting [J]. Transactions of Nonferrous Metals Society of China, 2017, 27(4): 829−838.

[18] ISMAEEL A, WANG Cun-shan. Effect of Nb additions on microstructure and properties of γ-TiAl based alloys fabricated by selective laser melting [J]. Transactions of Nonferrous Metals Society of China, 2019, 29(5): 1007−1016.

[19] MARTIN J H, YAHATA B D, HUNDLEY J M, MAYER J A, SCHAEDLER T A, POLLOCK T M. 3D printing of high-strength aluminium alloys [J]. Nature, 2017, 549(7672): 365−369.

[20] TOTTEN G E, MACKENZIE D S. Handbook of aluminum: Vol. 1. Physical metallurgy and processes [M]. New York: CRC Press, 2003.

[21] SANTOS M C, MACHADO A R, SALES W F, BARROZO M A S, EZUGWU E O. Machining of aluminum alloys: A review [J]. The International Journal of Advanced Manufacturing Technology, 2016, 86(9−12): 3067−3080.

[22] CHAKRABARTI D J, LAUGHLIN D E. Phase relations and precipitation in Al−Mg−Si alloys with Cu additions [J]. Progress in Materials Science, 2004, 49(3−4): 389−410.

[23] BARTKOWIAK K, ULLRICH S, FRICK T, SCHMIDT M. New developments of laser processing aluminium alloys via additive manufacturing technique [J]. Physics Procedia, 2011, 12: 393−401.

[24] KRUTH J P, LEVY G, KLOCKE F, CHILDS T H C. Consolidation phenomena in laser and powder-bed based layered manufacturing [J]. CIRP Annals−Manufacturing Technology, 2007, 56(2): 730−759.

[25] LIU R, WANG Z, SPARKS T, LIOU F, NEWKIRK J. Aerospace applications of laser additive manufacturing [C]//Laser Additive Manufacturing 2017. Cambridge: Woodhead Publishing, 2017: 351−371.

[26] JIA Qing-bo, ROMETSCH P, KUERNSTEINER P, CHAO Qi, HUANG Ai-jun, WEYLAND M, BOURGEOIS L, WU Xin-hua. Selective laser melting of a high strength Al−Mn−Sc alloy: Alloy design and strengthening mechanisms [J]. Acta Materialia, 2019, 171: 108−118.

[27] LIU Y J, LIU Z, JIANG Y, WANG G W, YANG Y, ZHANG L C. Gradient in microstructure and mechanical property of selective laser melted AlSi10Mg [J]. Journal of Alloys and Compounds, 2018, 735: 1414−1421.

[28] FORTUNATO A, LULAJ A, MELKOTE S, LIVERANI E, ASCARI A, UMBRELLO D. Milling of maraging steel components produced by selective laser melting [J]. The International Journal of Advanced Manufacturing Technology, 2017, 94(5−8): 1895−1902.

[29] BUCHBINDER D, SCHLEIFENBAUM H, HEIDRICH S, MEINERS W, BUELTMANN J. High power selective laser melting (HP SLM) of aluminum parts [J]. Physics Procedia, 2011, 12: 271−278.

[30] ZHANG Jin-liang, SONG Bo, WEI Qing-song, BOURELL D, SHI Yu-sheng. A review of selective laser melting of aluminum alloys: Processing, microstructure, property and developing trends [J]. Journal of Materials Science & Technology, 2019, 35(2): 270−284.

[31] OLAKANMI E O, COCHRANE R F, DALGARNO K W. A review on selective laser sintering/melting (SLS/SLM) of aluminium alloy powders: Processing, microstructure, and properties [J]. Progress in Materials Science, 2015, 74: 401−477.

[32] PRASHANTH K G, SCUDINO S, KLAUSS H J, SURREDDI K B, LOEBER L, WANG Z, CHAUBEY A K, KUEHN U, ECKERT J. Microstructure and mechanical properties of Al−12Si produced by selective laser melting: Effect of heat treatment [J]. Materials Science and Engineering A, 2014, 590: 153−160.

[33] PRASHANTH K G, SCUDINO S, MAITY T, DAS J, ECKERT J. Is the energy density a reliable parameter for materials synthesis by selective laser melting? [J]. Materials Research Letters, 2017, 5(6): 386−390.

[34] KIM Dong-kyu, WOO Wanchuck, HWANG Ji-hyun, AN Ke, CHOI Shi-hoon. Stress partitioning behavior of an AlSi10Mg alloy produced by selective laser melting during tensile deformation using in situ neutron diffraction [J]. Journal of Alloys and Compounds, 2016, 686: 281−286.

[35] READ N, WANG Wei, ESSA K, ATTALLAH M M. Selective laser melting of AlSi10Mg alloy: Process optimisation and mechanical properties development [J]. Materials & Design, 2015, 65: 417−424.

[36] HITZLER L, MERKEL M, HALL W, OECHSNER A. A review of metal fabricated with laser- and powder-bed based additive manufacturing techniques: Process, nomenclature, materials, achievable properties, and its utilization in the medical sector [J]. Advanced Engineering Materials, 2018, 20(5): 1700658.

[37] ZHANG Hu, ZHU Hai-hong, QI Ting, HU Zhi-heng, ZENG Xiao-yan. Selective laser melting of high strength Al−Cu−Mg alloys: Processing, microstructure and mechanical properties [J]. Materials Science and Engineering A, 2016, 656: 47−54.

[38] WANG Pei, GAMMER C, BRENNE F, PRASHANTH K G, MENDES R G, RUEMMELI M H, GEMMING T, ECKERT J, SCUDINO S. Microstructure and mechanical properties of a heat-treatable Al−3.5Cu−1.5Mg−1Si alloy produced by selective laser melting [J]. Materials Science and Engineering A, 2018, 711: 562−570.

[39] CROTEAU J R, GRIFFITHS S, ROSSELL M D, LEINENBACH C, KENEL C, JANSEN V, SEIDMAN D N, DUNAND D C, VO N Q. Microstructure and mechanical properties of Al−Mg−Zr alloys processed by selective laser melting [J]. Acta Materialia, 2018, 153: 35−44.

[40] SPIERINGS A B, DAWSON K, HEELING T, UGGOWITZER P J, SCHAEUBLIN R, PALM F, WEGENER K. Microstructural features of Sc- and Zr-modified Al−Mg alloys processed by selective laser melting [J]. Materials & Design, 2017, 115: 52−63.

[41] WANG P, LI H C, PRASHANTH K G, ECKERT J, SCUDINO S. Selective laser melting of Al−Zn−Mg−Cu: Heat treatment, microstructure and mechanical properties [J]. Journal of Alloys and Compounds, 2017, 707: 287−290.

[42] SUN Si-yu, LIU Peng, HU Jia-ying, HONG Chang, QIAO Xue, LIU Si-yu, ZHANG Rui-yun, WU Cheng-ge. Effect of solid solution plus double aging on microstructural characterization of 7075 Al alloys fabricated by selective laser melting (SLM) [J]. Optics & Laser Technology, 2019, 114: 158−163.

[43] KAUFMANN N, IMRAN M, WISCHEROPP T M, EMMELMANN C, SIDDIQUE S, WALTHER F. Influence of process parameters on the quality of aluminium alloy EN AW 7075 using selective laser melting (SLM) [J]. Physics Procedia, 2016, 83: 918−926.

[44] ASKELAND D R, FULAY P P, WRIGHT W J. The science and engineering of materials [M]. 6th ed. United States: Cengage Learning, 2010.

[45] SPIGARELLI S, PAOLETTI C. A new model for the description of creep behaviour of aluminium-based composites reinforced with nanosized particles [J]. Composites Part A: Applied Science and Manufacturing, 2018, 112: 346−355.

[46] LIU Pei, WANG Ai-qin, XIE Jing-pei, HAO Shi-ming. Characterization and evaluation of interface in SiC_p/2024 Al composite [J]. Transactions of Nonferrous Metals Society of China, 2015, 25(5): 1410−1418.

[47] DONG Cui-ge, CUI Rui, WANG Ri-chu, PENG Chao-qun, CAI Zhi-yong. Microstructures and mechanical properties of Al 2519 matrix composites reinforced with Ti-coated SiC particles [J]. Transactions of Nonferrous Metals Society of China, 2020, 30(4): 863−871.

[48] IBRAHIM I A, MOHAMED F A, LAVERNIA E J. Particulate reinforced metal matrix composites—A review [J]. Journal of Materials Science, 1991, 26(5): 1137−1156.

[49] ERVINA EFZAN M N, SITI SYAZWANI N, AL BAKRI ABDULLAH M M. Fabrication method of aluminum matrix composite (AMCs): A review [J]. Key Engineering Materials, 2016, 700: 102−110.

[50] WANG Zhi, QU R T, SCUDINO S, SUN B A, PRASHANTH K G, LOUZGUINE-LUZGIN D V, CHEN M W, ZHANG Z F, ECKERT J. Hybrid nanostructured aluminum alloy with super-high strength [J]. NPG Asia Materials, 2015, 7(12): e229.

[51] YU P, ZHANG L C, ZHANG W Y, DAS J, KIM K B, ECKERT J. Interfacial reaction during the fabrication of $Ni_{60}Nb_{40}$ metallic glass particles-reinforced Al based MMCs [J]. Materials Science and Engineering A, 2007, 444(1−2): 206−213.

[52] MAVHUNGU S T, AKINLABI E T, ONITIRI M A, VARACHIA F M. Aluminum matrix composites for industrial use: Advances and trends [J]. Procedia Manufacturing, 2017, 7: 178−182.

[53] SRIVATSAN T S, SUDARSHAN T S, LAVERNIA E J. Processing of discontinuously-reinforced metal matrix composites by rapid solidification [J]. Progress in Materials

Science, 1995, 39(4−5): 317−409.

[54] TORRALBA J M, DA COSTA C E, VELASO F. P/M aluminum matrix composites: An overview [J]. Journal of Materials Processing Technology, 2003, 133(1): 203−206.

[55] LI Hai-chao, WANG Pei, JIA Yan-dong, YU Zhi-shui, CHEN Qiang, SCUDINO S. Heat treatable Al−Zn−Mg−Cu matrix composites reinforced with Ni−based metallic glass powder [J]. Advanced Engineering Materials, 2019, 21(7): 1900021.

[56] RAMANATHAN A, KRISHNAN P K, MURALIRAJA R. A review on the production of metal matrix composites through stir casting−Furnace design, properties, challenges, and research opportunities [J]. Journal of Manufacturing Processes, 2019, 42: 213−245.

[57] MAZAHERY A, SHABANI M O. Characterization of cast A356 alloy reinforced with nano SiC composites [J]. Transactions of Nonferrous Metals Society of China, 2012, 22(2): 275−280.

[58] BAINS P S, SIDHU S S, PAYAL H S. Fabrication and machining of metal matrix composites: A review [J]. Materials and Manufacturing Processes, 2015, 31(5): 553−573.

[59] ZHOU Dong-shuai, QIU Feng, WANG Hui-yuan, JIANG Qi-chuan. Manufacture of nano-sized particle-reinforced metal matrix composites: A review [J]. Acta Metallurgica Sinica (English Letters), 2014, 27(5): 798−805.

[60] LU Ti-wen, CHEN Wei-ping, XU Wei-ye, WANG Pei, MAO Meng-di, LIU Yi-xiong, FU Zhi-qiang. The effects of Cr particles addition on the aging behavior and mechanical properties of SiC_p/7075Al composites [J]. Materials Characterization, 2018, 136: 264−271.

[61] ABBASIPOUR B, NIROUMAND B, MONIR VAGHEFI S M. Compocasting of A356-CNT composite [J]. Transactions of Nonferrous Metals Society of China, 2010, 20(9): 1561−1566.

[62] SERCOMBE T B, LI X. Selective laser melting of aluminium and aluminium metal matrix composites: Review [J]. Materials Technology, 2016, 31(2): 77−85.

[63] YOUSSEF Y M, DASHWOOD R J, LEE P D. Effect of clustering on particle pushing and solidification behaviour in TiB_2 reinforced aluminium PMMCs [J]. Composites Part A: Applied Science and Manufacturing, 2005, 36(6): 747−763.

[64] OZDEN S, EKICI R, NAIR F. Investigation of impact behaviour of aluminium based SiC particle reinforced metal-matrix composites [J]. Composites Part A: Applied Science and Manufacturing, 2007, 38(2): 484−494.

[65] REQUENA G, YUBERO D C, CORROCHANO J, REPPER J, GARCES G. Stress relaxation during thermal cycling of particle reinforced aluminium matrix composites [J]. Composites Part A: Applied Science and Manufacturing, 2012, 43(11): 1981−1988.

[66] DEBROY T, WEI H L, ZUBACK J S, MUKHERJEE T, ELMER J W, MILEWSKI J O, BEESE A M, WILSON-HEID A, DE A, ZHANG W. Additive manufacturing of metallic components−Process, structure and properties [J]. Progress in Materials Science, 2018, 92: 112−224.

[67] KOU S. Welding metallurgy [M]. 2nd ed. New Jersey: John Wiley & Sons, Inc., 2003.

[68] CHEN Shi-jia, GUILLEMOT G, GANDIN CHARLES A. Three-dimensional cellular automaton-finite element modeling of solidification grain structures for arc-welding processes [J]. Acta Materialia, 2016, 115: 448−467.

[69] LIU Shi-wen, ZHU Hai-hong, PENG Gang-yong, YIN Jie, ZENG Xiao-yan. Microstructure prediction of selective laser melting AlSi10Mg using finite element analysis [J]. Materials & Design, 2018, 142: 319−328.

[70] LI Xu-xiao, TAN Wen-da. Numerical investigation of effects of nucleation mechanisms on grain structure in metal additive manufacturing [J]. Computational Materials Science, 2018, 153: 159−169.

[71] KURZ W, FISHER D J. Fundamentals of solidification [M]. 4th ed. Zurich: Trans Tech Publications, 1989.

[72] THIJS L, KEMPEN K, KRUTH J P, van HUMBEECK J. Fine-structured aluminium products with controllable texture by selective laser melting of pre-alloyed AlSi10Mg powder [J]. Acta Materialia, 2013, 61(5): 1809−1819.

[73] LI Jing, CHENG Xu, LI Zhuo, ZONG Xiao, ZHANG Shu-quan, WANG Hua-ming. Improving the mechanical properties of Al−5Si−1Cu−Mg aluminum alloy produced by laser additive manufacturing with post-process heat treatments [J]. Materials Science and Engineering A, 2018, 735: 408−417.

[74] LEI Qian, RAMAKRISHNAN B P, WANG Shu-juan, WANG Yi-chen, MAZUMDER J, MISRA A. Structural refinement and nanomechanical response of laser remelted Al−Al_2Cu lamellar eutectic [J]. Materials Science and Engineering A, 2017, 706: 115−125.

[75] PAULY S, WANG Pei, KUEHN U, KOSIBA K. Experimental determination of cooling rates in selectively laser-melted eutectic Al−33Cu [J]. Additive Manufacturing, 2018, 22: 753−757.

[76] DINDA G P, DASGUPTA A K, MAZUMDER J. Evolution of microstructure in laser deposited Al−11.28%Si alloy [J]. Surface and Coatings Technology, 2012, 206(8−9): 2152−2160.

[77] RAO Heng, GIET S, YANG Kun, WU Xin-hua, DAVIES C H J. The influence of processing parameters on aluminium alloy A357 manufactured by selective laser melting [J]. Materials & Design, 2016, 109: 334−346.

[78] RAI A, HELMER H, KOERNER C. Simulation of grain structure evolution during powder bed based additive manufacturing [J]. Additive Manufacturing, 2017, 13: 124−134.

[79] YUAN Peng-peng, GU Dong-dong, DAI Dong-hua. Particulate migration behavior and its mechanism during selective laser melting of TiC reinforced Al matrix nanocomposites [J]. Materials & Design, 2015, 82: 46−55.

[80] GAN Zheng-tao, LIU Hao, LI Shao-xia, HE Xiu-li, YU Gang. Modeling of thermal behavior and mass transport in multi-layer laser additive manufacturing of Ni-based alloy on cast iron [J]. International Journal of Heat and Mass Transfer, 2017, 111: 709−722.

[81] TAN J H, WONG W L E, DALGARNO K W. An overview of powder granulometry on feedstock and part performance in the selective laser melting process [J]. Additive Manufacturing, 2017, 18: 228−255.

[82] LI Ya-li, GU Dong-dong. Thermal behavior during selective laser melting of commercially pure titanium powder: Numerical simulation and experimental study [J]. Additive Manufacturing, 2014, 1−4: 99−109.

[83] GUSAROV A V, SMUROV I. Modeling the interaction of laser radiation with powder bed at selective laser melting [J]. Physics Procedia, 2010, 5: 381−394.

[84] GUSAROV A V, YADROITSEV I, BERTRAND P H, SMUROV I. Model of radiation and heat transfer in laser-powder interaction zone at selective laser melting [J]. Journal of Heat Transfer, 2009, 131(7): 072101.

[85] LIU Yang, YANG Yong-qiang, MAI Shu-zhen, WANG Di, SONG Chang-hui. Investigation into spatter behavior during selective laser melting of AISI 316L stainless steel powder [J]. Materials & Design, 2015, 87: 797−806.

[86] ZHAO C, FEZZAA K, CUNNINGHAM R W, WEN H, de CARLO F, CHEN L, ROLLETT A D, SUN T. Real-time monitoring of laser powder bed fusion process using high-speed X-ray imaging and diffraction [J]. Scientific Reports, 2017, 7(1): 3602.

[87] KHAIRALLAH S A, ANDERSON A. Mesoscopic simulation model of selective laser melting of stainless steel powder [J]. Journal of Materials Processing Technology, 2014, 214(11): 2627−2636.

[88] LI Rui-di, LIU Jin-hui, SHI Yu-sheng, WANG Li, JIANG Wei. Balling behavior of stainless steel and nickel powder during selective laser melting process [J]. The International Journal of Advanced Manufacturing Technology, 2011, 59(9−12): 1025−1035.

[89] GU Dong-dong, ZHANG Hong-mei, DAI Dong-hua, XIA Mu-jian, HONG Chen, POPRAWE R. Laser additive manufacturing of nano-TiC reinforced Ni-based nanocomposites with tailored microstructure and performance [J]. Composites Part B: Engineering, 2019, 163: 585−597.

[90] WANG P, DENG L, PRASHANTH K G, PAULY S, ECKERT J, SCUDINO S. Microstructure and mechanical properties of Al−Cu alloys fabricated by selective laser melting of powder mixtures [J]. Journal of Alloys and Compounds, 2018, 735: 2263−2266.

[91] LOH L E, CHUA C K, YEONG W Y, SONG J, MAPAR M, SING S L, LIU Z H, ZHANG D Q. Numerical investigation and an effective modelling on the selective laser melting (SLM) process with aluminium alloy 6061 [J]. International Journal of Heat and Mass Transfer, 2015, 80: 288−300.

[92] DAI Dong-hua, GU Dong-dong, POPRAWE R, XIA Mu-jian. Influence of additive multilayer feature on thermodynamics, stress and microstructure development during laser 3D printing of aluminum-based material [J]. Science Bulletin, 2017, 62(11): 779−787.

[93] DONG H B, LEE P D. Simulation of the columnar-to-equiaxed transition in directionally solidified Al−Cu alloys [J]. Acta Materialia, 2005, 53(3): 659−668.

[94] PRASHANTH K G, SCUDINO S, CHAUBEY A K, LOEBER L, WANG Pei, ATTAR H, SCHIMANSKY F P, PYCZAK F, ECKERT J. Processing of Al−12Si−TNM composites by selective laser melting and evaluation of compressive and wear properties [J]. Journal of Materials Research, 2015, 31(1): 55−65.

[95] KANG Nan, FU Ying-qing, CODDET P, GUELORGET Bruno, LIAO Han-lin, CODDET C. On the microstructure, hardness and wear behavior of Al−Fe−Cr quasicrystal reinforced Al matrix composite prepared by selective laser melting [J]. Materials & Design, 2017, 132: 105−111.

[96] GENG J W, HONG T R, MA Yu, WANG M L, CHEN Dong, MA N H, WANG H W. The solution treatment of in-situ sub-micron TiB_2/2024 Al composite [J]. Materials & Design, 2016, 98: 186−193.

[97] TIAN Kang-le, ZHAO Yu-tao, JIAO Lei, ZHANG Song-li, ZHANG Zhen-ya, WU Xiu-chuan. Effects of in situ generated ZrB_2 nano-particles on microstructure and tensile properties of 2024Al matrix composites [J]. Journal of Alloys and Compounds, 2014, 594: 1−6.

[98] ASTHANA R. Reinforced cast metals. Part I: Solidification microstructure [J]. Journal of Materials Science, 1998, 33(7): 1679−1698.

[99] MONTERO SISTIAGA M L, MERTENS R, VRANCKEN B, WANG X B, van HOOREWEDER B, KRUTH J P, van HUMBEECK J. Changing the alloy composition of Al7075 for better processability by selective laser melting [J]. Journal of Materials Processing Technology, 2016, 238: 437−445.

[100] MARCANTONIO J A, MONDOLFO L F. Grain refinement in aluminum alloyed with titanium and boron [J]. Metallurgical Transactions, 1971, 2(2): 465−471.

[101] YAN Fu-yao, XIONG Wei, FAIERSON E. Grain structure control of additively manufactured metallic materials [J]. Materials, 2017, 10(11): 1260.

[102] SMALLMAN R E, NGAN A H W. Solidification [C]//Modern Physical Metallurgy 2014. Amsterdam: Elsevier, 2014: 93−119.

[103] AZIZ M J. Model for solute redistribution during rapid solidification [J]. Journal of Applied Physics, 1982, 53(2): 1158−1168.

[104] ZHANG H, ZHU H H, NIE X J, YIN J, HU Z H, ZENG X Y. Effect of Zirconium addition on crack, microstructure and mechanical behavior of selective laser melted Al−Cu−Mg alloy [J]. Scripta Materialia, 2017, 134: 6−10.

[105] XIAO Y K, BIAN Z Y, WU Y, JI G, LI Y Q, LI M J, LIAN Q, CHEN Z, ADDAD A, WANG H W. Effect of nano-TiB_2 particles on the anisotropy in an AlSi10Mg alloy processed by selective laser melting [J]. Journal of Alloys and Compounds, 2019, 798: 644−655.

[106] HAN Yan-feng, DAI Yong-bing, SHU Da, WANG Jun, SUN Bao-de. First-principles calculations on the stability of

Al/TiB_2 interface [J]. Applied Physics Letters, 2006, 89(14): 144107.

[107] SUN Jing, WANG Xu-qin, CHEN Yan, WANG Fei, WANG Hao-wei. Effect of Cu element on morphology of TiB_2 particles in TiB_2/Al−Cu composites [J]. Transactions of Nonferrous Metals Society of China, 2020, 30(5): 1148−1156.

[108] XI L, KABAN I, NOWAK R, KORPALA B, BRUZDA G, SOBCZAK N, MATTERN N, ECKERT J. High-temperature wetting and interfacial interaction between liquid Al and TiB_2 ceramic [J]. Journal of Materials Science, 2015, 50(7): 2682−2690.

[109] XI L X, WANG P, PRASHANTH K G, LI H, PRYKHODKO H V, SCUDINO S, KABAN I. Effect of TiB_2 particles on microstructure and crystallographic texture of Al−12Si fabricated by selective laser melting [J]. Journal of Alloys and Compounds, 2019, 786: 551−556.

[110] XI L X, ZHANG H, WANG P, LI H C, PRASHANTH K G, LIN K J, KABAN I, GU D D. Comparative investigation of microstructure, mechanical properties and strengthening mechanisms of Al−12Si/TiB_2 fabricated by selective laser melting and hot pressing [J]. Ceramics International, 2018, 44(15): 17635−17642.

[111] ATTAR H, BOENISCH M, CALIN M, ZHANG L C, ZHURAVLEVA K, FUNK A, SCUDINO S, YANG C, ECKERT J. Comparative study of microstructures and mechanical properties of in situ Ti−TiB composites produced by selective laser melting, powder metallurgy, and casting technologies [J]. Journal of Materials Research, 2014, 29(17): 1941−1950.

[112] XI Li-xia, GU Dong-dong, GUO Shuang, WANG Rui-qi, DING Kai, PRASHANTH K G. Grain refinement in laser manufactured Al-based composites with TiB_2 ceramic [J]. Journal of Materials Research and Technology, 2020, 9(3): 2611−2622.

[113] ALMANGOUR B, GRZESIAK D, YANG Jenn-ming. Selective laser melting of TiC reinforced 316L stainless steel matrix nanocomposites: Influence of starting TiC particle size and volume content [J]. Materials & Design, 2016, 104: 141−151.

[114] ALMANGOUR B, GRZESIAK D, YANG Jenn-ming. Selective laser melting of TiB_2/H13 steel nanocomposites: Influence of hot isostatic pressing post-treatment [J]. Journal of Materials Processing Technology, 2017, 244: 344−353.

[115] GU Dong-dong, WANG Hong-qiao, ZHANG Guo-quan. Selective laser melting additive manufacturing of Ti-based nanocomposites: The role of nanopowder [J]. Metallurgical and Materials Transactions A, 2013, 45(1): 464−476.

[116] SONG Bo, DONG Shu-juan, CODDET P, ZHOU Gen-shu, OUYANG Sheng, LIAO Han-lin, CODDET C. Microstructure and tensile behavior of hybrid nano-micro SiC reinforced iron matrix composites produced by selective laser melting [J]. Journal of Alloys and Compounds, 2013, 579: 415−421.

[117] GU Dong-dong, YUAN Peng-peng. Thermal evolution behavior and fluid dynamics during laser additive manufacturing of Al-based nanocomposites: Underlying role of reinforcement weight fraction [J]. Journal of Applied Physics, 2015, 118(23): 233109.

[118] SURAPPA M K. Aluminium matrix composites: Challenges and opportunities [J]. Sadhana, 2003, 28(1): 319−334.

[119] LI Ying-li, ZHOU Kun, TOR Shu-beng, CHUA Chee-kai, LEONG Kah-fai. Heat transfer and phase transition in the selective laser melting process [J]. International Journal of Heat and Mass Transfer, 2017, 108: 2408−2416.

[120] DING Xue-ping, WANG Lin-zhi. Heat transfer and fluid flow of molten pool during selective laser melting of AlSi10Mg powder: Simulation and experiment [J]. Journal of Manufacturing Processes, 2017, 26: 280−289.

[121] DAYAL R, GAMBARYAN-ROISMAN T. Heat transfer in granular medium for application to selective laser melting: A numerical study [J]. International Journal of Thermal Sciences, 2017, 113: 38−50.

[122] LIAO Hai-long, ZHU Hai-hong, XUE Gang, ZENG Xiao-yan. Alumina loss mechanism of Al_2O_3−AlSi10 Mg composites during selective laser melting [J]. Journal of Alloys and Compounds, 2019, 785: 286−295.

[123] HAN Quan-quan, SETCHI R, LACAN F, GU Dong-dong, EVANS S L. Selective laser melting of advanced Al−Al_2O_3 nanocomposites: Simulation, microstructure and mechanical properties [J]. Materials Science and Engineering A, 2017, 698: 162−173.

[124] YOUNG T. An essay on the cohesion of fluids. [J]. Phil Trans Roy Soc, 1805, 95: 65−87.

[125] SOBCZAK N, SINGH M, ASTHANA R. High-temperature wettability measurements in metal/ceramic systems-Some methodological issues [J]. Current Opinion in Solid State and Materials Science, 2005, 9(4−5): 241−253.

[126] GU Dong-dong, RAO Xiang-wei, DAI Dong-hua, MA Cheng-long, XI Li-xia, LIN Kai-jie. Laser additive manufacturing of carbon nanotubes (CNTs) reinforced aluminum matrix nanocomposites: Processing optimization, microstructure evolution and mechanical properties [J]. Additive Manufacturing, 2019, 29: 100801.

[127] WANG Min, SONG Bo, WEI Qing-song, SHI Yu-sheng. Improved mechanical properties of AlSi7Mg/nano-SiC_p composites fabricated by selective laser melting [J]. Journal of Alloys and Compounds, 2019, 810: 151926.

[128] WANG P, GAMMER C, BRENNE F, NIENDORF T, ECKERT J, SCUDINO S. A heat treatable TiB_2/Al−3.5Cu−1.5Mg−1Si composite fabricated by selective laser melting: Microstructure, heat treatment and mechanical properties [J]. Composites Part B: Engineering, 2018, 147: 162−168.

[129] LIN T C, CAO C, SOKOLUK M, JIANG L, WANG X, SCHOENUNG J M, LAVERNIA E J, LI X. Aluminum with dispersed nanoparticles by laser additive manufacturing [J]. Nature Communications, 2019, 10(1): 4124.

[130] GAO Chao-feng, XIAO Zhi-yu, LIU Zhong-qiang, ZHU Quan-li, ZHANG Wei-wen. Selective laser melting of nano-TiN modified AlSi10Mg composite powder with low laser reflectivity [J]. Materials Letters, 2019, 236: 362−365.

[131] GAO C, WANG Z, XIAO Z, YOU D, WONG K, AKBARZADEH A H. Selective laser melting of TiN nanoparticle-reinforced AlSi10Mg composite: Microstructural, interfacial, and mechanical properties [J]. Journal of Materials Processing Technology, 2020, 281: 116618.

[132] TAN Hua, HAO Da-peng, AL-HAMDANI K, ZHANG Feng-ying, XU Zheng-kai, CLARE A T. Direct metal deposition of TiB_2/AlSi10Mg composites using satellited powders [J]. Materials Letters, 2018, 214: 123−126.

[133] SCIPIONI B U, WOLFER A J, MATTHEWS M J, DELPLANQUE J R, SCHOENUNG J M. On the limitations of volumetric energy density as a design parameter for selective laser melting [J]. Materials & Design, 2017, 113: 331−340.

[134] GUSTMANN T, NEVES A, KUEHN U, GARGARELLA P, KIMINAMI C S, BOLFARINI C, ECKERT J, PAULY S. Influence of processing parameters on the fabrication of a Cu−Al−Ni−Mn shape-memory alloy by selective laser melting [J]. Additive Manufacturing, 2016, 11: 23−31.

[135] ATTAR H, BOENISCH M, CALIN M, ZHANG L C, SCUDINO S, ECKERT J. Selective laser melting of in situ titanium titanium boride composites: Processing, microstructure and mechanical properties [J]. Acta Materialia, 2014, 76: 13−22.

[136] SANDER J, HUFENBACH J, GIEBELER L, WENDROCK H, KUEHN U, ECKERT J. Microstructure and properties of FeCrMoVC tool steel produced by selective laser melting [J]. Materials & Design, 2016, 89: 335−341.

[137] GU D D, WANG H Q, DAI D H, YUAN P P, MEINERS W, POPRAWE R. Rapid fabrication of Al-based bulk-form nanocomposites with novel reinforcement and enhanced performance by selective laser melting [J]. Scripta Materialia, 2015, 96: 25−28.

[138] JUE Jiu-bin, GU Dong-dong, CHANG Kun, DAI Dong-hua. Microstructure evolution and mechanical properties of Al−Al_2O_3 composites fabricated by selective laser melting [J]. Powder Technology, 2017, 310: 80−91.

[139] ANESTIEV L A, FROYEN L. Model of the primary rearrangement processes at liquid phase sintering and selective laser sintering due to biparticle interactions [J]. Journal of Applied Physics, 1999, 86(7): 4008−4017.

[140] ABOULKHAIR N T, MASKERY I, TUCK C, ASHCROFT I, EVERITT N M. On the formation of AlSi10Mg single tracks and layers in selective laser melting: Microstructure and nano-mechanical properties [J]. Journal of Materials Processing Technology, 2016, 230: 88−98.

[141] YADROITSEV I, BERTRAND P H, SMUROV I. Parametric analysis of the selective laser melting process [J]. Applied Surface Science, 2007, 253(19): 8064−8069.

[142] METELKOVA J, KINDS Y, KEMPEN K, de FORMANOIR C, WITVROUW A, van HOOREWEDER B. On the influence of laser defocusing in selective laser melting of 316L [J]. Additive Manufacturing, 2018, 23: 161−169.

[143] PHILO A M, MEHRABAN S, HOLMES M, SILLARS S, SUTCLIFFE C J, SIENZ J, BROWN S G R, LAVERY N P. A pragmatic continuum level model for the prediction of the onset of keyholing in laser powder bed fusion [J]. The International Journal of Advanced Manufacturing Technology, 2018, 101(1−4): 697−714.

[144] LIU Y J, LI S J, WANG H L, HOU W T, HAO Y L, YANG R, SERCOMBE T B, ZHANG L C. Microstructure, defects and mechanical behavior of beta-type titanium porous structures manufactured by electron beam melting and selective laser melting [J]. Acta Materialia, 2016, 113: 56−67.

[145] WANG J C, LIU Y J, QIN P, LIANG S X, SERCOMBE T B, ZHANG L C. Selective laser melting of Ti−35Nb composite from elemental powder mixture: Microstructure, mechanical behavior and corrosion behavior [J]. Materials Science and Engineering A, 2019, 760: 214−224.

[146] WEI Kai-wen, WANG Ze-min, ZENG Xiao-yan. Preliminary investigation on selective laser melting of Ti−5Al−2.5Sn α-Ti alloy: From single tracks to bulk 3D components [J]. Journal of Materials Processing Technology, 2017, 244: 73−85.

[147] KHAIRALLAH S A, ANDERSON A T, RUBENCHIK A, KING W E. Laser powder-bed fusion additive manufacturing: Physics of complex melt flow and formation mechanisms of pores, spatter, and denudation zones [J]. Acta Materialia, 2016, 108: 36−45.

[148] QI Ting, ZHU Hai-hong, ZHANG Hu, YIN Jie, KE Lin-da, ZENG Xiao-yan. Selective laser melting of Al7050 powder: Melting mode transition and comparison of the characteristics between the keyhole and conduction mode [J]. Materials & Design, 2017, 135: 257−266.

[149] MILLS K C, KEENE B J, BROOKS R F, SHIRALI A. Marangoni effects in welding [J]. Philosophical Transactions−Royal Society of London Series A Mathematical Physical and Engineering Sciences, 1998, 356(1739): 911−925.

[150] HEIPLE C R, ROPER J R. Mechanism for minor element effect on GTA fusion zone geometry [J]. Welding Journal, 1982, 61(4): 97−102.

[151] HEIPLE C R, ROPER J R, STAGNER R T, ADEN R J. Surface active element effects on the shape of GTA, laser and electron beam welds [J]. Welding Research Supplement, 1983, 62(3): 72−77.

[152] SHI Xue-zhi, MA Shu-yuan, LIU Chang-meng, WU Qian-ru. Parameter optimization for Ti−47Al−2Cr−2Nb in selective laser melting based on geometric characteristics of single scan tracks [J]. Optics & Laser Technology, 2017, 90: 71−79.

[153] ATTAR H, PRASHANTH K G, ZHANG Lai-chang, CALIN M, OKULOV I V, SCUDINO S, YANG Chao, ECKERT J. Effect of powder particle shape on the properties of in situ Ti−TiB composite materials produced by selective laser melting [J]. Journal of Materials Science & Technology, 2015, 31(10): 1001−1005.

[154] ZHANG L C, XU J, MA E. Consolidation and properties of ball-milled $Ti_{50}Cu_{18}Ni_{22}Al_4Sn_6$ glassy alloy by equal channel angular extrusion [J]. Materials Science and Engineering A, 2006, 434(1−2): 280−288.

[155] OSHIMA T, ZHANG You-lin, HIROTA M, SUZUKI M, NAKAGAWA T. The effect of the types of mill on the flowability of ground powders [J]. Advanced Powder Technology, 1995, 6(1): 35−45.

[156] GU Dong-dong, WANG Zhi-yang, SHEN Yi-fu, LI Qin, LI Yu-fang. In-situ TiC particle reinforced Ti−Al matrix composites: Powder preparation by mechanical alloying and selective laser melting behavior [J]. Applied Surface Science, 2009, 255(22): 9230−9240.

[157] ALMANGOUR B, GRZESIAK D, YANG J M. Selective laser melting of TiB_2/316L stainless steel composites: The roles of powder preparation and hot isostatic pressing post-treatment [J]. Powder Technology, 2017, 309: 37−48.

[158] SURYANARAYANA C. Mechanical alloying and milling [J]. Progress in Materials Science, 2001, 46(1): 1−184.

[159] LI X P, JI G, CHEN Z, ADDAD A, WU Y, WANG H W, VLEUGELS J, van HUMBEECK J, KRUTH J P. Selective laser melting of nano-TiB_2 decorated AlSi10Mg alloy with high fracture strength and ductility [J]. Acta Materialia, 2017, 129: 183−193.

[160] SIMCHI A, GODLINSKI D. Effect of SiC particles on the laser sintering of Al−7Si−0.3Mg alloy [J]. Scripta Materialia, 2008, 59(2): 199−202.

[161] ANANDKUMAR R, ALMEIDA A, COLACO R, VILAR R, OCELIK V, de HOSSON J T M. Microstructure and wear studies of laser clad Al−Si/$SiC_{(p)}$ composite coatings [J]. Surface and Coatings Technology, 2007, 201(24): 9497−9505.

[162] ASTFALCK L C, KELLY G K, LI Xiao-peng, SERCOMBE T B. On the breakdown of SiC during the selective laser melting of aluminum matrix composites [J]. Advanced Engineering Materials, 2017, 19(8): 1600835.

[163] GU Dong-dong, CHANG Fei, DAI Dong-hua. Selective laser melting additive manufacturing of novel aluminum based composites with multiple reinforcing phases [J]. Journal of Manufacturing Science and Engineering, 2014, 137(2): 021010.

[164] URENA A, RODRIGO P, GIL L, ESCALERA M D, BALDONEDO J L. Interfacial reactions in an Al−Cu−Mg (2009)/SiC_w composite during liquid processing. Part II: Arc welding [J]. Journal of Materials Science, 2001, 36(2): 429−439.

[165] HUTTUNEN-SAARIVIRTA E. Microstructure, fabrication and properties of quasicrystalline Al−Cu−Fe alloys: A review [J]. Journal of Alloys and Compounds, 2004, 363(1−2): 154−178.

[166] MUKHOPADHYAY N K, UHLENWINKEL V, SRIVASTAVA V C. Synthesis and characterization of bulk Al−Cu−Fe based quasicrystals and composites by spray forming [J]. Journal of Materials Engineering and Performance, 2015, 24(6): 2172−2178.

[167] WANG Z, PRASHANTH K G, CHAUBEY A K, LOEBER L, SCHIMANSKY F P, PYCZAK F, ZHANG W W, SCUDINO S, ECKERT J. Tensile properties of Al−12Si matrix composites reinforced with TiAl-based particles [J]. Journal of Alloys and Compounds, 2015, 630: 256−259.

[168] CLEMENS H, WALLGRAM W, KREMMER S, GUETHER V, OTTO A, BARTELS A. Design of novel β-solidifying TiAl alloys with adjustable β/B2-phase fraction and excellent hot-workability [J]. Advanced Engineering Materials, 2008, 10(8): 707−713.

[169] QIN Peng, LIU Yu-jing, SERCOMBE T B, LI Yu-hua, ZHANG Chuan-wei, CAO Chong-de, SUN Hong-qi, ZHANG Lai-chang. Improved corrosion resistance on selective laser melting produced Ti−5Cu alloy after heat treatment [J]. ACS Biomaterials Science & Engineering, 2018, 4(7): 2633−2642.

[170] SHIRVANIMOGHADDAM K, KHAYYAM H, ABDIZADEH H, KARBALAEI AKBARI M, PAKSERESHT A H, ABDI F, ABBASI A, NAEBE M. Effect of B_4C, TiB_2 and $ZrSiO_4$ ceramic particles on mechanical properties of aluminium matrix composites: Experimental investigation and predictive modelling [J]. Ceramics International, 2016, 42(5): 6206−6220.

[171] LIU X, LIU Y, HUANG D, HAN Q, WANG X. Tailoring in-situ TiB_2 particulates in aluminum matrix composites [J]. Materials Science and Engineering A, 2017, 705: 55−61.

[172] HAN Yan-feng, LIU Xiang-fa, BIAN Xiu-fang. In situ TiB_2 particulate reinforced near eutectic Al−Si alloy composites [J]. Composites Part A: Applied Science and Manufacturing, 2002, 33(3): 439−444.

[173] ZHAO Min, WU Gao-hui, JIANG Long-tao, DOU Zuo-yong. Friction and wear properties of TiB_{2P}/Al composite [J]. Composites Part A: Applied Science and Manufacturing, 2006, 37(11): 1916−1921.

[174] SCHUMACHER P, GREER A L, WORTH J, EVANS P V, KEARNS M A, FISHER P, GREEN A H. New studies of nucleation mechanisms in aluminium alloys: Implications for grain refinement practice [J]. Materials Science and Technology, 2013, 14(5): 394−404.

[175] WITUSIEWICZ V T, BONDAR A A, HECHT U, REX S, VELIKANOVA T Y. The Al−B−Nb−Ti system I. Re-assessment of the constituent binary systems B−Nb and B−Ti on the basis of new experimental data [J]. Journal of Alloys and Compounds, 2008, 448(1−2): 185−194.

[176] EMAMY M, MAHTA M, RASIZADEH J. Formation of TiB_2 particles during dissolution of $TiAl_3$ in Al−TiB_2 metal matrix composite using an in situ technique [J]. Composites Science and Technology, 2006, 66(7−8): 1063−1066.

[177] GUO Q, JIANG L T, CHEN G Q, FENG D, SUN D L, WU G H. SEM and TEM characterization of the microstructure of post-compressed TiB_2/2024Al composite [J]. Micron, 2012, 43(2−3): 380−386.

[178] DADBAKHSH S, HAO L. Effect of layer thickness in selective laser melting on microstructure of Al/5wt.%Fe_2O_3 powder consolidated parts [J]. The Scientific World Journal, 2014, 2014: 106129.

[179] DADBAKHSH S, HAO Liang. In situ formation of particle reinforced al matrix composite by selective laser melting of Al/Fe_2O_3 powder mixture [J]. Advanced Engineering

Materials, 2012, 14(1−2): 45−48.

[180] DADBAKHSH S, HAO L. Effect of Al alloys on selective laser melting behaviour and microstructure of in situ formed particle reinforced composites [J]. Journal of Alloys and Compounds, 2012, 541: 328−334.

[181] DADBAKHSH S, HAO L, JERRARD P G E, ZHANG D Z. Experimental investigation on selective laser melting behaviour and processing windows of in situ reacted Al/Fe_2O_3 powder mixture [J]. Powder Technology, 2012, 231: 112−121.

[182] HAN Quan-quan, GENG Yan-quan, SETCHI R, LACAN F, GU Dong-dong, EVANS S L. Macro and nanoscale wear behaviour of Al−Al_2O_3 nanocomposites fabricated by selective laser melting [J]. Composites Part B: Engineering, 2017, 127: 26−35.

[183] KANG N, EL MANSORI M, LIN X, GUITTONNEAU F, LIAO H L, HUANG W D, CODDET C. In-situ synthesis of aluminum/nano-quasicrystalline Al−Fe−Cr composite by using selective laser melting [J]. Composites Part B: Engineering, 2018, 155: 382−390.

[184] GU Dong-dong, WANG Hong-qiao, DAI Dong-hua, CHANG Fei, MEINERS W, HAGEDORN Y C, WISSENBACH K, KELBASSA I, POPRAWE R. Densification behavior, microstructure evolution, and wear property of TiC nanoparticle reinforced AlSi10Mg bulk-form nanocomposites prepared by selective laser melting [J]. Journal of Laser Applications, 2015, 27(S1): S17003.

[185] GU Dong-dong, WANG Hong-qiao, CHANG Fei, DAI Dong-hua, YUAN Peng-peng, HAGEDORN Y C, MEINERS W. Selective laser melting additive manufacturing of TiC/AlSi10Mg bulk-form nanocomposites with tailored microstructures and properties [J]. Physics Procedia, 2014, 56: 108−116.

[186] CHANG Fei, GU Dong-dong, DAI Dong-hua, YUAN Peng-peng. Selective laser melting of in-situ Al_4SiC_4+SiC hybrid reinforced Al matrix composites: Influence of starting SiC particle size [J]. Surface and Coatings Technology, 2015, 272: 15−24.

[187] JUE Jiu-bin, GU Dong-dong. Selective laser melting additive manufacturing of in situ $Al_2Si_4O_{10}$/Al composites: Microstructural characteristics and mechanical properties [J]. Journal of Composite Materials, 2017, 51(4): 519−532.

[188] DAI Dong-hua, GU Dong-dong, XIA Mu-jian, MA Cheng-long, CHEN Hong-yu, ZHAO Tong, HONG Chen, GASSER A, POPRAWE R. Melt spreading behavior, microstructure evolution and wear resistance of selective laser melting additive manufactured AlN/AlSi10Mg nanocomposite [J]. Surface and Coatings Technology, 2018, 349: 279−288.

[189] DAI Dong-hua, GU Dong-dong. Influence of thermodynamics within molten pool on migration and distribution state of reinforcement during selective laser melting of AlN/AlSi10Mg composites [J]. International Journal of Machine Tools and Manufacture, 2016, 100: 14−24.

[190] ZHAO Xiao, SONG Bo, FAN Wen-rui, ZHANG Yuan-jie, SHI Yu-sheng. Selective laser melting of carbon/AlSi10Mg composites: Microstructure, mechanical and electronical properties [J]. Journal of Alloys and Compounds, 2016, 665: 271−281.

[191] JIANG L Y, LIU T T, ZHANG C D, ZHANG K, LI M C, MA T, LIAO W H. Preparation and mechanical properties of CNTs-AlSi10Mg composite fabricated via selective laser melting [J]. Materials Science and Engineering A, 2018, 734: 171−177.

[192] ZHOU Yan, DUAN Long-chen, WEN Shi-feng, WEI Qing-song, SHI Yu-sheng. Enhanced micro-hardness and wear resistance of Al−15Si/TiC fabricated by selective laser melting [J]. Composites Communications, 2018, 10: 64−67.

[193] PRASHANTH K G, SHAKUR SHAHABI H, ATTAR H, SRIVASTAVA V C, ELLENDT N, UHLENWINKEL V, ECKERT J, SCUDINO S. Production of high strength $Al_{85}Nd_8Ni_5Co_2$ alloy by selective laser melting [J]. Additive Manufacturing, 2015, 6: 1−5.

[194] KOLI D K, AGNIHOTRI G, PUROHIT R. A review on properties, behaviour and processing methods for Al-nano Al_2O_3 composites [J]. Procedia Materials Science, 2014, 6: 567−589.

[195] YANG Yan, CHEN Yang, ZHANG Jun-xi, GU Xin-hui, QIN Peng, DAI Nian-wei, LI Xiao-peng, KRUTH J P, ZHANG Lai-chang. Improved corrosion behavior of ultrafine-grained eutectic Al−12Si alloy produced by selective laser melting [J]. Materials & Design, 2018, 146: 239−248.

[196] CHEN Yang, ZHANG Jun-xi, GU Xin-hui, DAI Nian-wei, QIN Peng, ZHANG Lai-chang. Distinction of corrosion resistance of selective laser melted Al−12Si alloy on different planes [J]. Journal of Alloys and Compounds, 2018, 747: 648−658.

[197] WANG X J, ZHANG L C, FANG M H, SERCOMBE T B. The effect of atmosphere on the structure and properties of a selective laser melted Al−12Si alloy [J]. Materials Science and Engineering A, 2014, 597: 370−375.

[198] LI Wei, LI Shuai, LIU Jie, ZHANG Ang, ZHOU Yan, WEI Qing-song, YAN Chun-ze, SHI Yu-sheng. Effect of heat treatment on AlSi10Mg alloy fabricated by selective laser melting: Microstructure evolution, mechanical properties and fracture mechanism [J]. Materials Science and Engineering: A, 2016, 663: 116−125.

[199] KIMURA T, NAKAMOTO T, MIZUNO M, ARAKI H. Effect of silicon content on densification, mechanical and thermal properties of Al−*x*Si binary alloys fabricated using selective laser melting [J]. Materials Science and Engineering A, 2017, 682: 593−602.

[200] PRASHANTH K G, SCUDINO S, ECKERT J. Defining the tensile properties of Al−12Si parts produced by selective laser melting [J]. Acta Materialia, 2017, 126: 25−35.

[201] KANG Nan, CODDET P, LIAO Han-lin, BAUR T, CODDET C. Wear behavior and microstructure of hypereutectic Al−Si alloys prepared by selective laser melting [J]. Applied Surface Science, 2016, 378: 142−149.

[202] SAMUEL A M, GARZA-ELIZONDO G H, DOTY H W, SAMUEL F H. Role of modification and melt thermal treatment processes on the microstructure and tensile properties of Al−Si alloys [J]. Materials & Design, 2015, 80: 99−108.

[203] SCUDINO S, LIU G, SAKALIYSKA M, SURREDDI K B, ECKERT J. Powder metallurgy of Al-based metal matrix composites reinforced with β-Al_3Mg_2 intermetallic particles: Analysis and modeling of mechanical properties [J]. Acta Materialia, 2009, 57(15): 4529−4538.

[204] STARKE JR E A, STALEY J T. Application of modern aluminum alloys to aircraft [J]. Progress in Aerospace Sciences, 1996, 32(2): 131−172.

[205] DURSUN T, SOUTIS C. Recent developments in advanced aircraft aluminium alloys [J]. Materials & Design, 2014, 56: 862−871.

[206] CASATI R, LEMKE J N, ALARCON A Z, VEDANI M. Aging behavior of high-strength Al alloy 2618 produced by selective laser melting [J]. Metallurgical and Materials Transactions A, 2016, 48(2): 575−579.

[207] AHUJA B, KARG M, NAGULIN K Y, SCHMIDT M. Fabrication and characterization of high strength Al−Cu alloys processed using laser beam melting in metal powder bed [J]. Physics Procedia, 2014, 56: 135−146.

[208] WARD-CLOSE C M, MINOR R, DOORBAR P J. Intermetallic-matrix composites — A review [J]. Intermetallics, 1996, 4(3): 217−229.

[209] GIROT F A, QUENISSET J M, NASLAIN R. Discontinuously-reinforced aluminum matrix composites [J]. Composites Science and Technology, 1987, 30(3): 155−184.

[210] HARRIGAN W C. Commercial processing of metal matrix composites [J]. Materials Science and Engineering A, 1998, 244(1): 75−79.

[211] SHI Yun-jia, YANG Kun, KAIRY S K, PALM F, WU Xin-hua, ROMETSCH P A. Effect of platform temperature on the porosity, microstructure and mechanical properties of an Al−Mg−Sc−Zr alloy fabricated by selective laser melting [J]. Materials Science and Engineering A, 2018, 732: 41−52.

[212] JAYALAKSHMI S, GUPTA S, SANKARANARAYANAN S, SAHU S, GUPTA M. Structural and mechanical properties of $Ni_{60}Nb_{40}$ amorphous alloy particle reinforced Al-based composites produced by microwave-assisted rapid sintering [J]. Materials Science and Engineering A, 2013, 581: 119−127.

[213] SCUDINO S, LIU G, PRASHANTH K G, BARTUSCH B, SURREDDI K B, MURTY B S, ECKERT J. Mechanical properties of Al-based metal matrix composites reinforced with Zr-based glassy particles produced by powder metallurgy [J]. Acta Materialia, 2009, 57(6): 2029−2039.

[214] MUSSON N J, YUE T M. The effect of matrix composition on the mechanical properties of squeeze-cast aluminium alloy−Saffil metal matrix composites. [J]. Materials Science and Engineering A, 1991, 135: 237−242.

[215] JAYALAKSHMI S, KAILAS S V, SESHAN S. Tensile behaviour of squeeze cast AM100 magnesium alloy and its Al_2O_3 fibre reinforced composites [J]. Composites Part A: Applied Science and Manufacturing, 2002, 33(8): 1135−1140.

[216] LI X P, WANG X J, SAUNDERS M, SUVOROVA A, ZHANG L C, LIU Y J, FANG M H, HUANG Z H, SERCOMBE T B. A selective laser melting and solution heat treatment refined Al−12Si alloy with a controllable ultrafine eutectic microstructure and 25% tensile ductility [J]. Acta Materialia, 2015, 95: 74−82.

[217] TEE K L, LU L, LAI M O. In situ processing of Al−TiB2 composite by the stir-casting technique [J]. Journal of Materials Processing Technology, 1999, 89−90: 513−519.

[218] SURESH S, SHENBAG N, MOORTHI V. Aluminium−titanium diboride (Al−TiB_2) metal matrix composites: Challenges and opportunities [J]. Procedia Engineering, 2012, 38: 89−97.

[219] PRAMOD S L, BAKSHI S R, MURTY B S. Aluminum-based cast in situ composites: A review [J]. Journal of Materials Engineering and Performance, 2015, 24(6): 2185−2207.

[220] YANG Yi, WEN Shi-feng, WEI Qing-song, LI Wei, LIU Jie, SHI Yu-sheng. Effect of scan line spacing on texture, phase and nanohardness of TiAl/TiB_2 metal matrix composites fabricated by selective laser melting [J]. Journal of Alloys and Compounds, 2017, 728: 803−814.

[221] LI Wei, LI Ming, LIU Jie, YANG Yi, WEN Shi-feng, WEI Qing-song, YAN Chunze, SHI Yu-sheng. Microstructure control and compressive properties of selective laser melted Ti−43.5Al−6.5Nb−2Cr−0.5B alloy: Influence of reduced graphene oxide (RGO) reinforcement [J]. Materials Science and Engineering A, 2019, 743: 217−222.

[222] SURYAWANSHI J, PRASHANTH K G, SCUDINO S, ECKERT J, PRAKASH O M, RAMAMURTY U. Simultaneous enhancements of strength and toughness in an Al−12Si alloy synthesized using selective laser melting [J]. Acta Materialia, 2016, 115: 285−294.

[223] WANG Pei, GEBERT A, YAN Lei, LI Hai-chao, LAO Chang-shi, CHEN Zhang-wei, KOSIBA K, KUEHN U, SCUDINO S. Corrosion of Al−3.5Cu−1.5Mg−1Si alloy prepared by selective laser melting and heat treatment [J]. Intermetallics, 2020, 124: 106871.

[224] UZAN N E, SHNECK R, YEHESKEL O, FRAGE N. Fatigue of AlSi10Mg specimens fabricated by additive manufacturing selective laser melting (AM-SLM) [J]. Materials Science and Engineering A, 2017, 704: 229−237.

[225] XI Li-xia, GUO Shuang, GU Dong-dong, GUO Meng, LIN Kai-jie. Microstructure development, tribological property and underlying mechanism of laser additive manufactured submicro-TiB_2 reinforced Al-based composites [J]. Journal of Alloys and Compounds, 2020, 819: 152980.

[226] UZAN N E, SHNECK R, YEHESKEL O, FRAGE N. High-temperature mechanical properties of AlSi10Mg specimens fabricated by additive manufacturing using selective laser melting technologies (AM-SLM) [J]. Additive Manufacturing, 2018, 24: 257−263.

选区激光熔化成形颗粒增强铝基复合材料综述

王 沛[1,2], Jürgen ECKERT[3,4], Konda-gokuldoss PRASHANTH[3,5,6],
吴明伟[7], Ivan KABAN[2], 席丽霞[2,8], Sergio SCUDINO[2]

1. 深圳大学 增材制造研究所, 深圳 518060;
2. Institute for Complex Materials, IFW Dresden, D-01069 Dresden, Germany;
3. Erich Schmid Institute of Materials Science, Austrian Academy of Sciences, A-8700 Leoben, Austria;
4. Department of Materials Science, Montanuniversität Leoben, A-8700 Leoben, Austria;
5. Department of Mechanical and Industrial Engineering, Tallinn University of Technology, 19086 Tallinn, Estonia;
6. CBCMT, School of Mechanical Engineering, Vellore Institute of Technology, Vellore-632 014, Tamil Nadu, India;
7. 台北科技大学 材料及资源工程系, 台北 10608;
8. 南京航空航天大学 材料科学与技术学院, 南京 210016

摘 要：选区激光熔化(SLM)是一种新兴逐层增材制造技术，能够生成具有三维复杂结构的高性能构件。颗粒增强铝基复合材料(PAMCs)由于结合铝基体和增强相的优异特性在很多领域被认为是一种重要材料。基于 SLM 和 PAMCs 的综合优势，新型 SLM PAMCs 在近年来被陆续开发和研究。因而，本文总结当前有关 SLM PAMCs 的研究进展。首先，着重分析 SLM PAMCs 的凝固行为。其次，对高性能 SLM PAMCs 设计和制造中涉及的重要问题进行全面的讨论，其中包括增强相的选择、工艺参数对成形和微观结构的影响以及缺陷演变和相调控。第三，对 SLM PAMCs 的性能和增强机制进行系统讨论。最后，对高性能 SLM PAMCs 未来发展方向提出建设性的观点。

关键词：选区激光熔化；铝基复合材料；凝固行为；显微组织；性能

(Edited by Bing YANG)